Check for updates

Increasing impact of North Atlantic Ocean circulation on sedimentary processes along the passive Galicia Margin (NW Spain) over the past 40 million years

Julia Haberkern[1,2,3]*[†], Till J. J. Hanebuth[2,4], Volkhard Spiess[2,3] and Tilmann Schwenk[2,3]

[1]Fraunhofer Institute for Wind Energy Systems, Bremerhaven, Germany, [2]MARUM—Center for Marine Environmental Sciences, University of Bremen, Bremen, Germany, [3]Faculty of Geosciences, University of Bremen, Bremen, Germany, [4]Department of Marine Science, Coastal Carolina University, Conway, SC, United States

Off the Northwestern Iberian Peninsula, the vigorous bottom-current regime interacts with a complex seafloor topography inside the Galicia Interior Basin (GIB), which was tectonically shaped during the opening of the North Atlantic Ocean basin in Cretaceous times. The evolving North Atlantic Ocean circulation determined the depositional pattern of the basin fill over time, which can, in turn, be utilized as palaeoceanographic archive. This study reconstructs the evolution of the GIB sedimentary system since the mid-Eocene, namely, resulting from interplay between down- and along-slope sediment-transport processes, using high-resolution multichannel seismic data. Six major depositional stages are identified and connected to the evolution of the North Atlantic Ocean circulation. 1) Levelling of topography shows that the influence of contourparallel bottom currents on the depositional pattern steadily intensified since the mid-Eocene; 2) The strengthening of Northern Component Water (NCW), associated with the opening of the Faeroe-Shetland Basin in the late Eocene, is documented along the southwestern European continental margin for the first time by the onset of a plastered contourite drift; 3) A shift in the depocenters provide evidence that the closure of the Tethys-Indian Seaway led to Tethys Outflow Water into the Atlantic Ocean at intermediate ocean depths in the Miocene; 4) Until the mid-Miocene, the tectonic stress regime initially associated with the Pyrenean Orogeny and the following Betic Orogeny led to both sets of small-scale faulting systems as well as submarine mass wasting indicated by slope scarps and mass-transport deposits; 5) The onset of modern-style Mediterranean Outflow Water (MOW) after the Messinian Salinity Crisis (5.3 Ma) caused a distinct change in the depositional dynamics from combined along- and down-slope transport processes towards predominantly contouritic deposition, which is evident from the construction of several separated

mounded contouritic drifts that formed during Pliocene and early Pleistocene times; and 6) The contourite drift growth continued during the middle and late Pleistocene, but under a gaining influence of down-slope processes.

1 Introduction

With the evolution of the paleo-ocean circulation since the opening of the North Atlantic Ocean basin in the Cretaceous, two factors still need to be understood: the formation of deep-water masses at the northern high latitudes as a key element of the Atlantic Meridional Overturning Circulation (AMOC) and the role the emerging Mediterranean Outflow Water (MOW) has played (Pérez-Asensio et al., 2012; Rogerson et al., 2012). Palaeoceanographic proxies have been used to unravel the evolution of the North Atlantic Ocean circulation over geologic times (e.g., Woodruff and Savin, 1989; Wright et al., 1992; Stille et al., 1996; Bartoli et al., 2005; Scher and Martin, 2008; Abelson and Erez, 2017; Coxall et al., 2018). Contourite drifts, as long-lived deep-sea sediment depocenters induced by geostrophic bottom currents, record the presence, direction, and strength of bottom currents. Therefore, the existence, geometry, and architecture of contourite drifts have been proven as a powerful alternative for unravelling over-regional consequences of the opening or closure of major seaways related to regional tectonics or sea-level changes (Knutz, 2008, and references therein; Dutkiewicz and Müller, 2022). For the North Atlantic Ocean system, the onset of contourite drift formation at high latitudes (e.g., Feni, Eirik, Gloria drifts; Mienert et al., 1994; Uenzelmann-Neben and Gruetzner, 2018) captured the opening timing of the Norwegian-Greenland Seaways in Paleozoic to early Eocene times (Miller et al., 2009; Coxall et al., 2018). The following onset of high-density water formation enhancing AMOC from 40 to 34 Ma and the associated North Atlantic Deep Water (NADW) production has been reflected by the initiation of the south-eastern Faeroe Drift in association with the opening of the Faeroe-Shetland Basin around 35 Ma (Scher and Martin, 2004; Davies et al., 2001; Hovikoski ety al., 2021). Further south, the Gulf of Cadiz contourite system has recorded the ultimate opening of the Gibraltar Strait and the onset of the MOW at around 3.5 Ma (Stow et al., 2013; Hernández-Molina et al., 2014).

This study focuses on the passive continental margin off Galicia (NW Spain), where contourite drift deposits have generally been present since the Pliocene (Nisancioglu et al., 2003; Hernández-Molina et al., 2014; 2016) and formed under the influence of both the North Atlantic deep-water masses and MOW in glacial times (Hanebuth et al., 2015; Zhang et al., 2016b; Petrovic et al., 2019). The utilized high-resolution multichannel seismic dataset resolves the late Paleogene and Neogene depositional succession in sufficient resolution to differentiate the imprint of major remote seaway dynamics that have taken place since late Eocene times (past 40 Ma). In this study the major changes in sediment deposition observed in the seismic data are linked to changes in the oceanographic regime to infer ages for the deposits. Furthermore, the dense lateral data coverage also allows for distinguishing the effects of distinct regional tectonic phases on sedimentation pattern along the submarine part of the continental margin during the Neogene. It further illustrates phases of down-slope sediment transport and the specific interaction between the evolving bottom-current regime with the local seabed topography.

2 Settings

2.1 Geology of the Galicia Continental Margin

The Galicia Continental Margin is characterized by the presence of an intra-slope basin, the Galicia Interior Basin (GIB; Figure 1; Murillas et al., 1990; Munoz et al., 2003; Druet et al., 2018). This structural basin of almost 3,000 m water depth is separated from the Iberian Abyssal Plain by the Galicia Bank, a structural high peaking up to less than 700 m water depth (Ercilla et al., 2008; López-Pérez et al., 2021). The Galicia continental margin represents the eastern flank of GIB and extends from 100 to 2,800 m water depth (Figure 1A). The overall evolution of the regional topography was controlled by several phases of tectonic activity. GIB formed during early North Atlantic rifting in late Jurassic/early Cretaceous times, initiating the ultimate opening of the North Atlantic Ocean basin (Murillas et al., 1990). GIB poses an example of rifting of thin and cold crust, which led to necking and sequential faulting, subsequently resulting in a horst and graben system with tilted blocks (Pérez-Gussinyé et al., 2003; Brune et al., 2017; Druet et al., 2018; Sandoval et al., 2019; King et al., 2020). Early deposits, that accumulated inside GIB directly after its opening, indicate shallow-marine conditions that existed prior to and during the rifting phase (Murillas et al., 1990; Sutra and Manatschal, 2012). The modern maximum water depth of 3,000 m resulted from major subsidence in the Late Cretaceous after the basin continued to widen (Galice et al., 1979; Sutra and Manatschal, 2012; Sandoval et al., 2019). Syn-rift deposition in Lower Cretaceous times was associated with deformation, tilting, and mass-wasting processes (Murillas et al., 1990). The mode of syn-rift deposition lasted until the late Aptian and was bound by a distinct regional stratigraphic unconformity west of the Galicia Bank, which indicates the ultimate breakup of the North Atlantic Ocean basin. The post-rift sequence cored at the Vigo Seamount South of GIB seems not to show any significant tectonic influence and is bound by a stratigraphic hiatus from Albian to Campanian times attributed to an early deep-ocean circulation regime that established in Early-Upper Cretaceous times (Murillas et al., 1990).

GIB has repeatedly been subject to regional tectonic stress regimes over Paleogene and Neogene times. During the mid-Eocene, the *Pyrenean Orogeny* exerted an N-S compressional regime, which affected large topographic structures and caused small-scale faulting, folding, and inverted-graben formation offshore NW
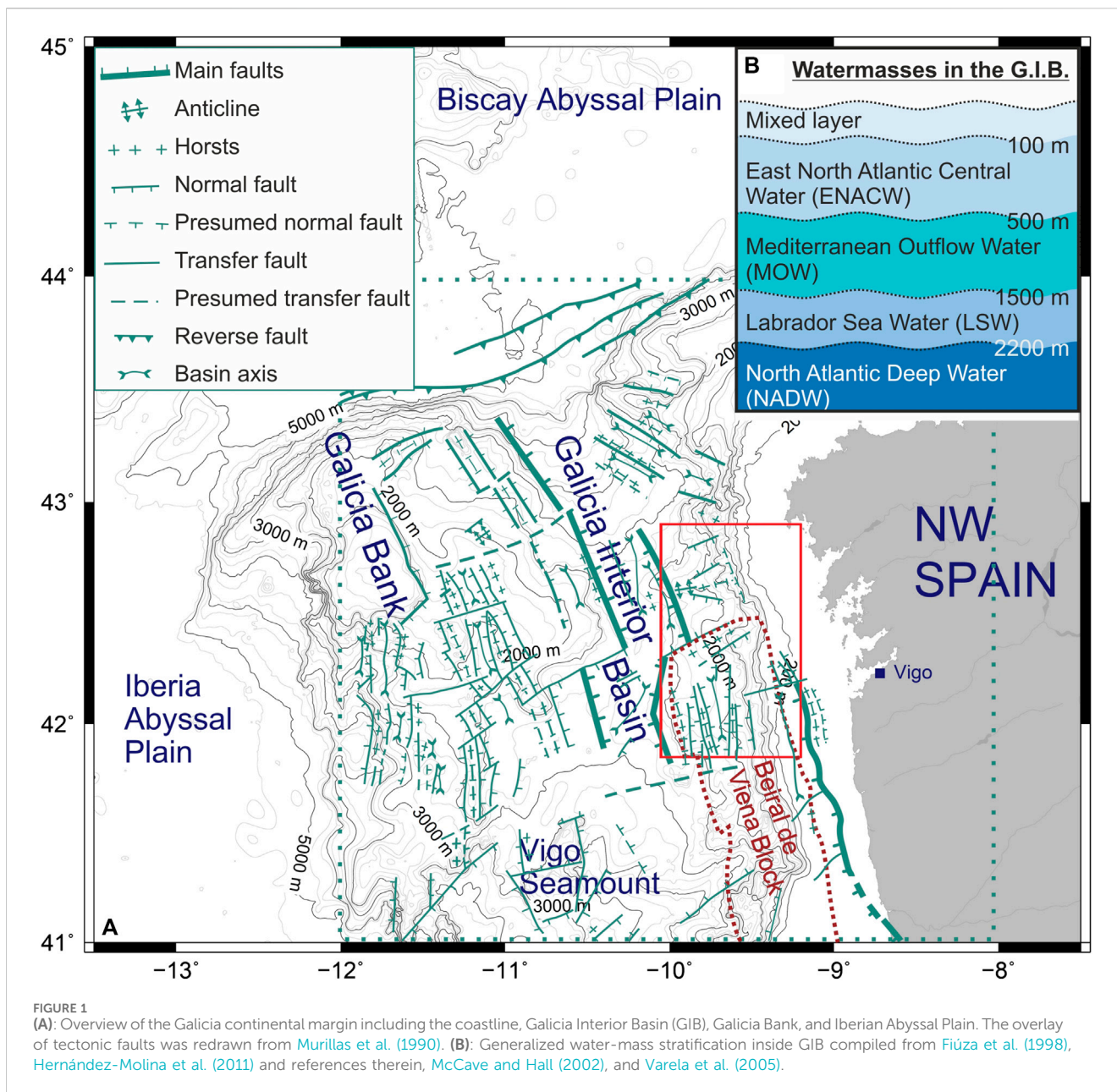
FIGURE 1
(A): Overview of the Galicia continental margin including the coastline, Galicia Interior Basin (GIB), Galicia Bank, and Iberian Abyssal Plain. The overlay of tectonic faults was redrawn from Murillas et al. (1990). **(B)**: Generalized water-mass stratification inside GIB compiled from Fiúza et al. (1998), Hernández-Molina et al. (2011) and references therein, McCave and Hall (2002), and Varela et al. (2005).

Iberia (Muñoz et al., 2003; Vázquez et al., 2008; Martín-González et al., 2011), as the Iberian and Eurasian continents collided with rotational dynamics and oceanic crust was subducted in the Bay of Biscay (Le Pichon and Sibuet, 1971; Boillot et al., 1979; Vázquez et al., 2008). Local structural features inside GIB, such as a local topographic height and an anticline (Obstacle OB1 and Ridge RD1 in this study; Figure 2B) experienced uplift during this period (Murillas et al., 1990).

In the early Miocene, renewed compressional stress resulted from the convergence of Iberia and Africa during the *Betic Orogeny*, which affected large parts of western Iberia tectonically by reactivating the Variscan fault system, Early Cretaceous rift faults, and elements of the preceding Pyrenean Orogeny (Galice et al., 1979; Muñoz et al., 2003). The uplift of the Beiral de Viena Block at the eastern flank of GIB (Figure 1A) led to an overall reduction in basin width (Muñoz et al., 2003), when previous faults

and folds were reactivated, remaining active until recent times (Murillas et al., 1990; Muñoz et al., 2003). Information on the history of post-rift sediment dynamics inside GIB is, however, sparse. While Boillot et al. (1979) suggested hemipelagic conditions during Paleogene and Neogene times, Murillas et al. (1990) discovered slide and contourite deposits as well. A similar diversity of sedimentary processes and products was described for the adjacent Galicia Bank for the post-rift phase (Ercilla et al., 2008).

2.2 Quaternary sediment dynamics at the Galicia Continental Margin

Quaternary and recent sediment dynamics are, in contrast, comparably well understood. The continental sediment has mainly
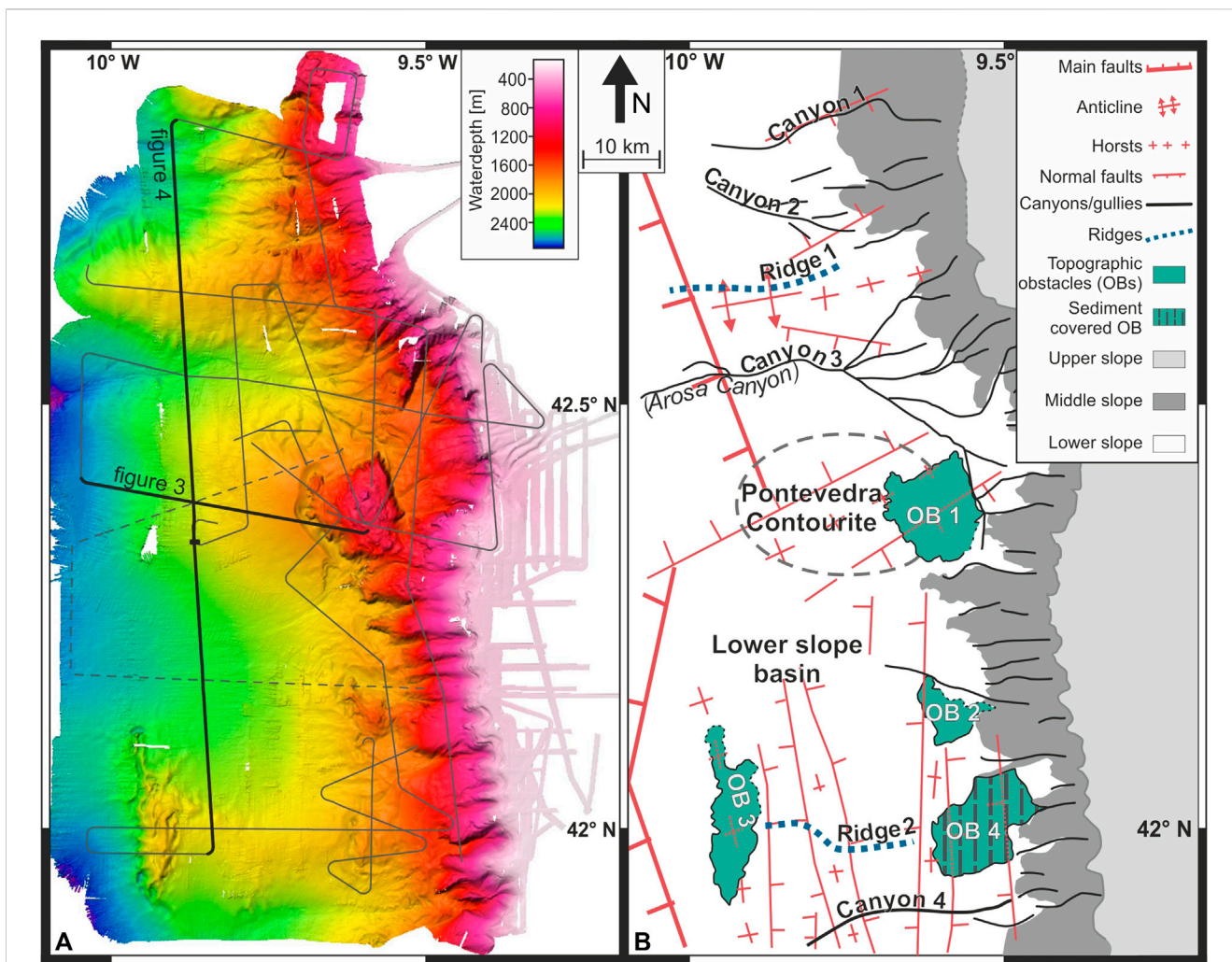
FIGURE 2
(A): Bathymetric map of the study area (modified from Hanebuth et al., 2015) showing the location of seismic lines; hachured lines originate from the POS342 dataset. Thick lines represent the seismic profiles shown in Figures 3, 4. **(B)**: Interpreted bathymetry, highlighting the outline of upper, middle, and lower continental slope as well as major submarine morphological features. The overlay of tectonic faults is redrawn from Murillas et al. (1990).

been supplied from Portuguese rivers. While large amounts of sand have accumulated on the outer shelf, fine-grained material has intermittently been stored in a mid-shelf mudbelt (Dias et al., 2002a; 2002b; Lantzsch et al., 2009; 2010; Oberle et al., 2014a; Zhang et al., 2016a). Resuspension during storm events has been allowed for efficient off-shelf transport in bottom nepheloid layers (Dias et al., 2002b; Oliveira et al., 2002; Vitorino et al., 2002; Oberle et al., 2014b). Sediment deposition at the continental slope and inside GIB has been governed by a succession of hemipelagic deposition, the arrival of ice-rafted debris, phases of contouritic activity, and down-slope processes (Hall and McCave, 2000; Bender et al., 2012; Martins et al., 2013; Hanebuth et al., 2015; Zhang et al., 2016b; Plaza-Morlote et al., 2017; Mena et al., 2018; Petrovic et al., 2019). Both downslope and along-slope sedimentation has particularly been sensitive to major oceanographic changes from glacial to interglacial stages, with elevated sedimentation rates during lower sea levels as the river mouths were located near the shelf break (Dias et al., 2002b; Lantzsch et al., 2010; Bender et al., 2012; Hanebuth et al., 2015), changing current intensities and vertical extensions of NADW,

Labrador Sea Water (LSW), and MOW (Schönfeld and Zahn, 2000; Varela et al., 2005; Voelker et al., 2006).

2.3 Modern oceanographic situation along the Galicia Continental Margin

Today, five main water masses flow northward along the continental slope (Figure 1B). The mixed surface water extends down to 100 m water depth (Fiúza et al., 1998; McCave and Hall, 2002; Varela et al., 2005). The underlying East North Atlantic Central Water (ENACW) shows two cores of highest current velocity between 300 and 500 m (Fiúza et al., 1998; McCave and Hall, 2002). MOW is split into two cores as well, the depths of which have alternatively been described at 500–700 m for the upper core and 800 to 1,400 m for the lower (Hernández-Molina et al., 2011, and references therein) and around 800 m for the upper and 1,100 m for the lower core (Fiúza et al., 1998; Varela et al., 2005). LSW is present at 1,500 to 2,300 m. The deepest water mass is NADW, which extends down to 4,000 m in

the abyssal plain off the Galicia Bank (Fiúza et al., 1998; Hernández-Molina et al., 2011, and references therein). As MOW and LSW have existed only since the Pliocene (3.8–3.5 Ma; Hernández-Molina et al., 2014), this configuration prevailed for less than 4 % of the 140-Ma long history of North Atlantic Ocean circulation.

2.4 Evolution of the North Atlantic Ocean circulation

2.4.1 Evolution—Establishment of the Atlantic Meridional Overturning (AMOC)

In the initial early and mid-Cretaceous, North Atlantic Ocean circulation was characterized by stratified, comparably warm, and saline bottom waters that formed at low latitudes due to the warm global climate (Roth, 1986; Coxall et al., 2018). Global surface and intermediate water-mass circulation patterns followed circum-equatorial pathways through the Central American Seaway, the new North Atlantic Ocean basin, and the Mediterranean/Tethys basins (Sewall et al., 2007; Torfstein and Steinberg, 2020). With the widening of the South Atlantic Ocean basin in Late to Latest Cretaceous times, deep water started to form at southern high latitudes and was able to reach the North Atlantic Ocean basin in the Campanian (79–75 Ma) due to the deepening of the Central Atlantic Gateway, until a significant latitudinal water exchange between the two Atlantic Ocean basins was established around 59 Ma (mid-Paleocene) (Murphy and Thomas, 2013; Donnadieu et al., 2016; Batenburg et al., 2018; Torfstein and Steinberg, 2020; Dutkiewicz and Müller, 2022).

Defined deep- and bottom-water masses were limited to the North Atlantic and Tethys Oceans; the oceans were generally poorly ventilated during the outgoing Mesozoic (Roth, 1986; Miller et al., 2009; Straume et al., 2020). Bottom-water ventilation improved with the deepening of the South Atlantic Ocean basin due to an intensification of southern high-latitude deep-water formation in Late Cretaceous times (Robinson and Vance, 2012) and a further intensification of the South Atlantic circulation in the early Paleogene (Palcu et al., 2020). The onset of Northern Component Water (NCW), the ancient equivalent of NADW, represents the initiation of deep-water production at North Atlantic high latitudes at around 35 Ma (Priabonian/latest Eocene), as indicated by an onset of the Southeast Faeroes Drift in the Faeroe-Shetland Basin (Davies et al., 2001; Poore et al., 2006; Langton et al., 2016; Coxall et al., 2018; Hovikoski et al., 2021). An early influence of NCW has been detected at the Walvis Ridge 33 Ma ago (Rupelian/Earliest Oligocene), demonstrating that this water mass had spread across both connected Atlantic Ocean basins by then (Via and Thomas, 2006).

The opening of the Drake Passage between South America and western Antarctica initiated in the mid-Eocene (Barthonian; Scher and Martin, 2006; Lagabrielle et al., 2009; Tremblin et al., 2016; Pérez-Díaz and Eagles, 2017; Coxall et al., 2018; Dutkiewicz and Müller, 2022). Its subsequent deepening from 25 to 20 Ma (Chattian-earliest Burdigalian/latest Oligocene-early Miocene) induced a major reorganization of the global ocean-current system as the modern Southern Ocean circum-Antarctic current system was able to establish (Stille et al., 1996; Langton et al., 2016; Straume et al., 2020).

2.4.2 Tethys Atlantic exchange

In the Cretaceous, general deep-water transport was directed eastward (Trabucho Alexandre et al., 2010), with the exception of a Tethyan outflow of deep and intermediate water into the Atlantic via the Pyrenean Corridor (Liu et al., 2023). Overall Tethyan circulation was characterized by a warm westward flowing surface current (Jovane et al., 2009; de la Vara and Meijer, 2016; Liu et al., 2023) Deep or intermediate Atlantic water entered the Tethys ocean, forming an estuarine exchange pattern of water masses (Pucéat et al., 2005; Trabucho Alexandre et al., 2010; de la Vara and Meijer, 2016). The surface current reportedly weakened during the Eocene (Hernández-Molina et al., 2022) or is even considered to have shut down by the end of the Eocene (33.55 Ma) (Jovane et al., 2004; Jovane et al., 2009). This likely preceded the full closure of the equatorial Indian Ocean–Mediterranean Seaway, which is dated between 24 Ma (latest Oligocene; Torftstein and Steinberg, 2020) and 14 Ma (Langhian; Stille et al., 1996; Rögl, 1999; Dutkiewicz and Müller, 2022). The ocean-water exchange pattern between the semi-enclosed Tethys remnant ocean basin and the Atlantic Ocean basin during these times is still under debate. The most probable scenario would be an analogue to the modern anti-estuarine mode with an inflow of Atlantic surface water and an intermediate warm and salty outflow from the Tethys basins/paleo-Mediterranean Sea (Kouwenhoven and van der Zwaan, 2006; de la Vara and Meijer, 2016).

2.4.3 Iceland Faroe ridge and AMOC strengthening

The deepening of the Fram strait from 30 Ma onward can be associated with an increasing supply of Arctic deep water to the Norwegian Greenland Sea (Straume et al., 2020). NCW in the North Atlantic significantly intensified 16 Ma ago (Burdigalian-Langhian boundary/mid-Miocene), when a subsidence of the Iceland-Faeroe Ridge in the Norwegian-Greenland Seaway opened an additional pathway for bottom water masses forming in the Norwegian and Greenland Seas (Stille et al., 1996; Poore et al., 2006; Hovikoski et al., 2021). Consequently, the transport direction of bottom water within the combined Atlantic Ocean basins, that prevalently flew northward in late Mesozoic to early Miocene times, reversed at this time, having maintained a southward flow over the past 14 Ma (Woodruff and Savin, 1989).

2.4.4 Central American Seaway (CAS) and further AMOC strengthening

NCW circulation and AMOC further strengthened in the later mid-Miocene as a consequence of a progressive narrowing and shoaling of the Central American Seaway (CAS) (Nisancioglu et al., 2003; Bell et al., 2015; Montes et al., 2015; Alves et al., 2023). This was a prolonged and discontinuous process: the deep-water exchange through this equatorial ocean passage was largely restricted after 12 to 9 Ma; many studies date its closure around 3.8 to 3.5 Ma, while others provide a wider span of 4.2 to 2.4 Ma (Duque-Caro, 1990; Haug and Tiedemann, 1998; Karas et al., 2017). The review of O'Dea et al. (2016) states that at 3.2 Ma no relevant interoceanic water exchange between the Atlantic and Pacific oceans was possible through CAS, however the sensu strictu closure is dated to 2.8 Ma (O'Dea et al., 2016).

2.4.5 Strait of Gibraltar

Whilst the CAS was still shoaling and closing, the Strait of Gibraltar closed and reopened at 5.3 Ma, driving the Messinian salinity crisis (Hernández-Molina et al., 2014; Ng et al., 2021). An early influence of MOW appeared at 4.5 Ma (Rogerson et al., 2012; Hernández-Molina et al., 2014).

2.4.6 Modern (Pliocene/Quaternary) AMOC evolution

Also, LSW appeared in the north-east Atlantic Ocean around 4.5 Ma for the first time (Nisancioglu et al., 2003). NCW production decreased along with the general onset of northern hemisphere glaciation around 3.6 to 3.1 Ma (Bartoli et al., 2005), while NADW formation significantly enhanced after 2.7 Ma (latest Pliocene; Blake-Mizen et al., 2019; Hayashi et al., 2020). NCW formation, nevertheless, intensified during two subsequent time intervals, one coinciding with the Mid-Pleistocene Transition (MPT) 1.2 to 0.7 Ma ago and the second after 0.3 Ma (Poore et al., 2006), whereas MOW strengthened prior to the MPT and weakened afterwards (Hernández-Molina et al., 2014), suggesting a competing mechanism.

3 Materials and methods

This study is based on the interpretation of multibeam bathymetry and multichannel seismic (MCS) profiles. The main part of the dataset was acquired during cruise GALIOMAR III with the German R/V METEOR (M84-4; Hanebuth et al., 2012). The bathymetric map was produced by merging data from the two hull-mounted Kongsberg Simrad swath-sounding systems EM122 and EM710 into a 100-m resolution grid. Processing was carried out using the open-source software MB system and FLEDERMAUS (QPS).

Multichannel seismic data was acquired during the M84-4 cruise by shooting a GI Gun with a volume of 2 x 1.7 L every 7 seconds. The main emitted frequencies were in the range of 100–300 Hz. The signal was recorded with a 400-m long Syntron Streamer with 64 channels. The M84-4 multichannel seismic data set was complemented by three lines collected during the preceding cruise GALIOMAR I aboard the German R/V POSEIDON (POS342; Hanebuth et al., 2007). Those lines were acquired using a Mini GI-Gun with reduced chamber volumes (2 x 0.25 L) and a frequency range of 100–500 Hz. A 101-m long Teledyne streamer with 16 channels was used for the recording during POS342.

MCS data processing was performed using the Vista seismic processing suite (Schlumberger). The standard processing sequence included binning to an along-track resolution of 5 m, debiasing, trace editing, normal-moveout correction with a constant velocity of 1,500 m/s, static correction, filtering, and despiking prior to common-midpoint stacking. After stacking, white noise reduction and FD-migration were carried out.

For an integrated data interpretation, the software Kingdom (IHS Global Inc.) was used. Interpretation included picking and gridding of horizons as well as contour-line calculations. Thickness maps of seismic units between picked horizons were generated by subtracting the two-way travel time (TWT) reflected by major unit boundaries, resulting in true vertical-thickness maps. In contrast to true stratigraphic thickness, which is measured perpendicular to the

bedding, true vertical thickness may display too large thickness values at very steep slopes, an effect that had to be considered during the thickness interpretation in this study. Sedimentation rates for each seismic unit were estimated using the median thickness averaged over the entire lower continental slope in the study area. These values were converted from TWT into meters using a constant velocity of 1,500 m/s. The calculated sedimentation rates were additionally corrected for sediment compaction increasing with depth by using the equation and material constants for depth-dependent pore volume reduction after Sclater and Christie (1980). As muddy, sandy, and even gravelly late Quaternary deposits were sampled in the study area (Bender et al., 2012; Hanebuth et al., 2015), the material constants for sand have been chosen over shale and limestone to guarantee a conservative estimation of compaction and avoid overcompensation.

In the absence of any boreholes, finding ages for sedimentation rate had to be established through comparison of changes in the area to adjacent areas as well as major oceanographic changes. At least the two deepest horizons, H0 and H1, could be fixed in age through correlation with an overlapping lower resolution seismic line from Murillas et al. (1990). For the uppermost seismic units, comparison was possible with data from the Pontevedra Contourite (Hanebuth et al., 2015) Ages from six sediment cores covering a maximum timespan of 60 ka were averaged to sedimentation rates of 9.99 cm/ka. Due to the limited coverage and short timespan, this rate only served to crosscheck the order of magnitude for calculated sediment rates.
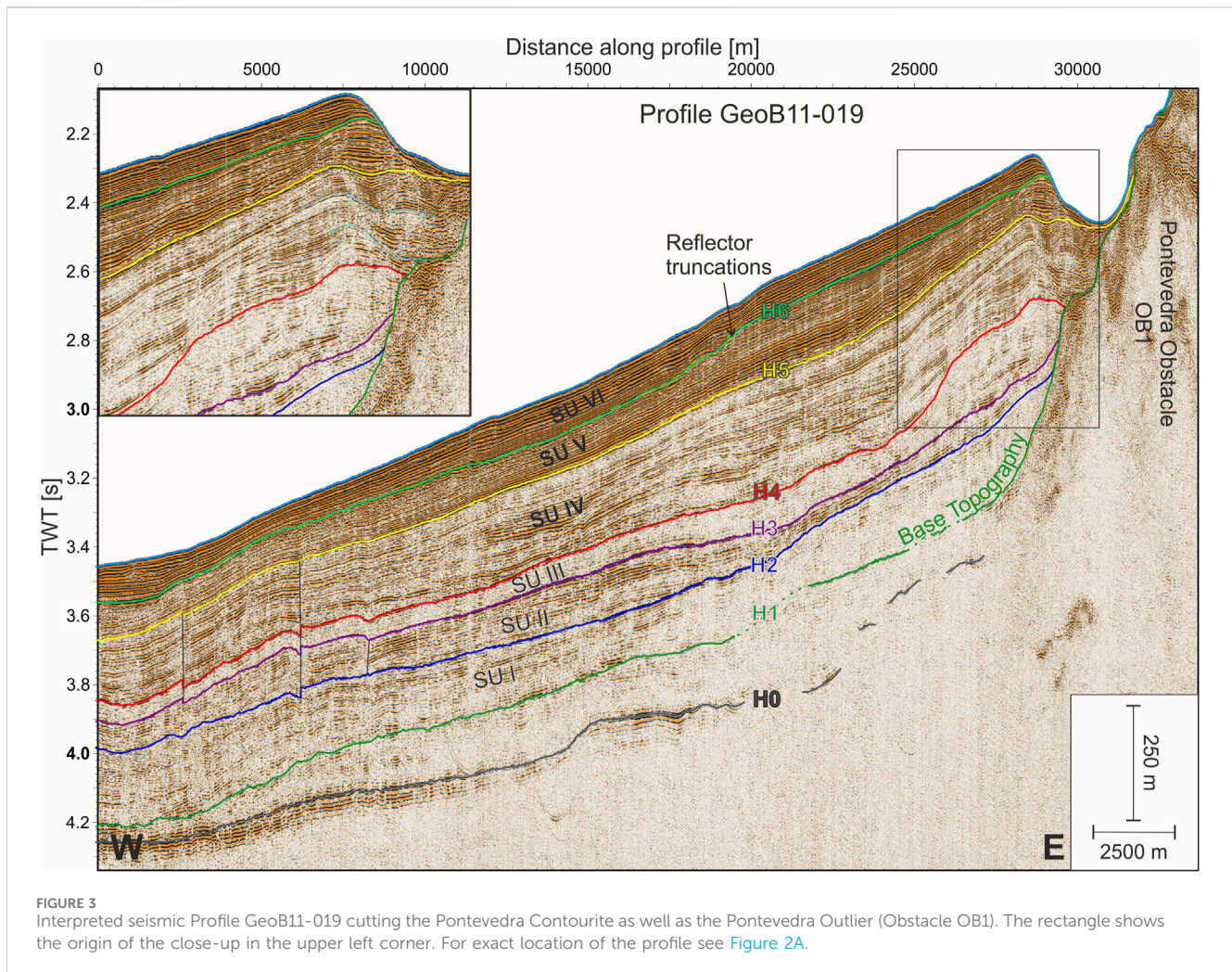
4 Results

4.1 Modern topographic elements

From east to west, the slope is divided into three physiographic zones (Figure 2B). The upper slope extends from the shelf break at 160–180 m down to 300 m water depth and is associated with a gradient generally lower than 3°. The middle slope extends down to water depths of 1,300 to 1,800 m, is characterized by a gradient of 8°–15°, and is dissected by dozens of gullies that cut back into the shelf edge. The lower slope extends to 2,800 m with a gentler gradient not exceeding 4°.

In the N-S direction, the lower slope is partitioned by several geomorphologic features. Four major *canyons* are present, which are each connected to one or more of the mid-slope gullies, and lead westwards into the deep GIB (Canyons CY 1 to CY4; Figure 2B). Two canyons (CY 1 and CY2) are located in the very north of the study area; the third canyon (CY3), named Arosa Canyon (Boillot et al., 1979), is situated about 20 km south, i.e., in the central part of the study area. The fourth (CY4) is located in the very south (Figure 2B). Two topographic *ridges* (RDs 1 and 2; Figure 2B) are located between Canyons CY2 and CY3 (RD1) and directly north of Canyon CY4 (RD2), respectively, in the form of elongated east-west trending, 15–20 km wide and up to 500 m high elevations. Four geographically isolated topographic *obstacles* (OB1 to OB4; Figure 2B) represent irregular-shaped heights with extremely steep flanks and a hummocky surface on top (Figure 1A). They are termed obstacles since they pose an obtrusion to water masses' flow. Obstacle OB1 is associated with a separated mounded contourite drift to its west, named 'Pontevedra Outlier' by Hanebuth et al.

FIGURE 3
Interpreted seismic Profile GeoB11-019 cutting the Pontevedra Contourite as well as the Pontevedra Outlier (Obstacle OB1). The rectangle shows the origin of the close-up in the upper left corner. For exact location of the profile see Figure 2A.

(2015) and Zhang et al. (2016b), and the drift is accordingly referred to as 'Pontevedra Contourite' in the following. An embayment on the lower slope, south of the Pontevedra Contourite and north of ridge RD2, is named 'Lower Slope Basin' in this study (Figure 2B).

Since the entire study area falls into the necking domain with a thin and brittle crust, the underlying topography is dominated by blocks of upper crust that faulted and tilted during rifting (Druet et al., 2018). The eastern continental slope of GIB shows two types of tectonic structuring, one stretching in an E-W and the other in an N-S directions (Figure 2A). The overlay of the interpreted bathymetry with a tectonic map compiled by Murillas et al. (1990) reveals a correlation of the majority of the topographic elements described above with deeper tectonic elements (Figure 2B). Ridge RD1 correlates with a structural combination of horst and anticline. Obstacle OB1 is located near another horst structure. The apparent offsets between the two maps can probably be attributed to deviations in geo-referencing.

It is noteworthy that the structural features in the northern part of the study area correlate with E-W trending faults, while the topographic obstacles in the south (OB2 to OB4) roughly coincide with N-S striking horst and graben systems. Small discrepancies of a few kilometers may again be induced by georeferencing uncertainties. Only Ridge RD2 does not correlate with any of the previously described deeper tectonic elements. The analysis of

sedimentary thickness distribution in the next paragraphs will show that it is indeed a sedimentary ridge.

4.2 Seismic facies and seismic units

The seismo-stratigraphic record is vertically separated by seven horizons (H0 to H6; Figure 3; 4; Table 1), which represent local unconformities often associated with changes in seismic facies. Six seismic facies (Facies A1, A2, B, C1, C2, D; Table 1) are defined following the classifications by Faugères et al. (1999) and Nielsen et al. (2008). The subdivision of the facies is based on reflection amplitude and internal reflection geometric pattern. In general, each facies is associated with contouritic drift dynamics, as no strictly horizontal or strictly parallel reflectors are identified, which would be indicative of turbiditic or hemipelagic deposition.

Seismic Facies A1 and A2 show a subparallel reflector configuration and are associated with sheeted contourite drifts of varying sediment composition; the higher amplitudes of Facies A1 might result from higher variability in grain size composition (Table 1). In comparison, the more contorted and laterally less continuous Facies B represents mainly sheeted drifts that were overprinted by post-depositional faulting or slope-creeping and
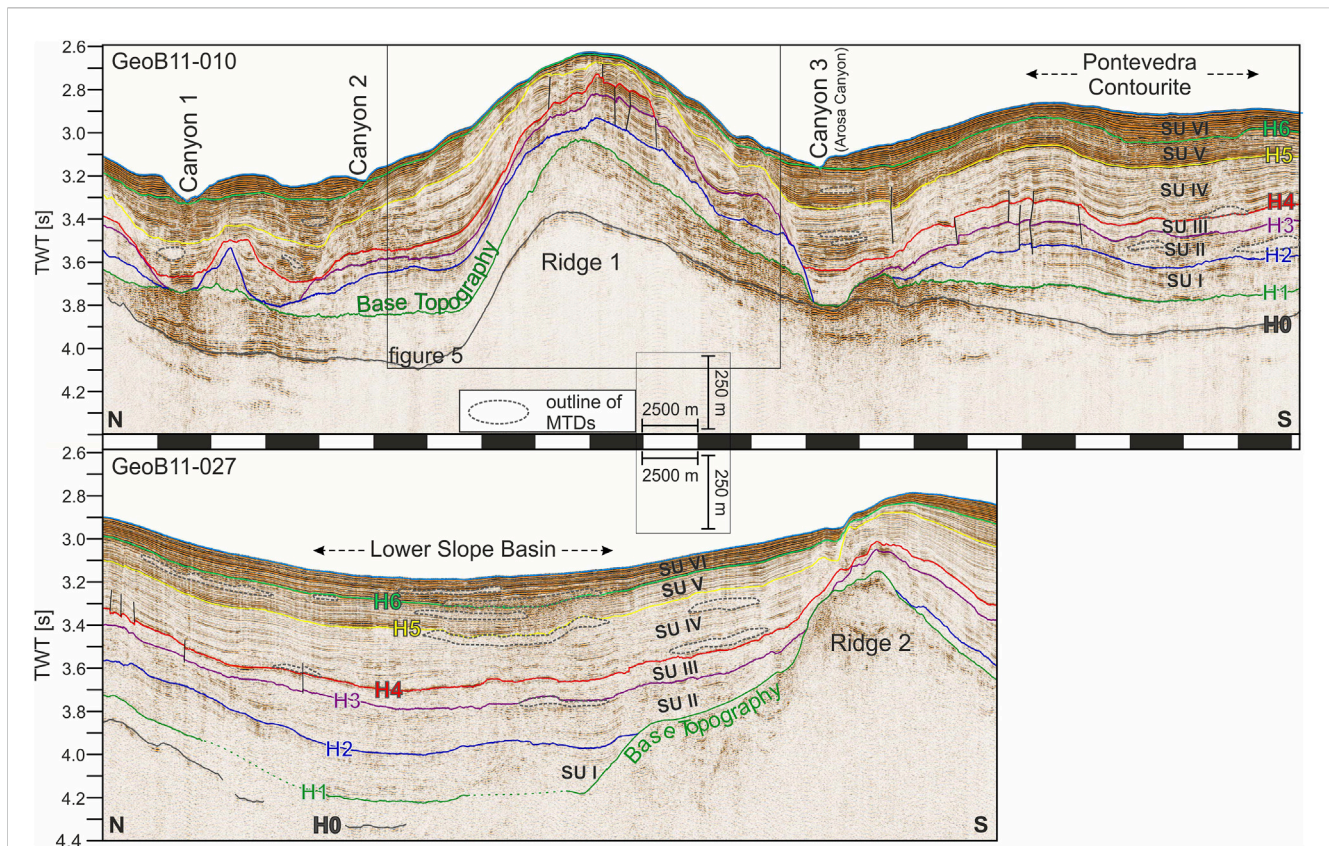
FIGURE 4
Interpreted seismic Profiles GeoB11-010 and GeoB11-027 crossing the study area in N-S direction (for exact location of the line see Figure 2A). Thereby the main structural features are crossed, including (from north to south): Canyons CY1 and CY2, Ridge RD1, Arosa Canyon, Pontevedra Contourite, Lower Slope Basin, and Ridge RD2. The dashed grey outlines indicate the location of MTDs. The most distinct faults are marked with thin black lines. The rectangle around Ridge 1 indicates the origin of the close-up shown in Figure 5.

might include minor mass-transport deposits (MTDs; Table 1). The post-depositional tectonic modification may have destroyed strictly horizontal/parallel layering, and it can, therefore, not be ruled out that turbidite or hemipelagite beds may have originally been part of this facies.

Facies C1 is characterized by a chaotic configuration and low amplitude; it represents MTDs that are thick enough to be individually separated in the seismic record (Table 1, e.g., Lower Slope Basin area of Figure 4). Facies C2, with its chaotic to contorted configuration and variable amplitudes, is associated with deposits whose internal structures underwent severe alteration during tectonically active phases. Facies C2 represents the seismic basement over wide areas and is particularly prominent at the topographic obstacles and the upper slope. Facies D represents contouritic drifts, which are associated with diverging reflectors as known for plastered and mounded drifts (following the classification of Faugères and Stow, 2008; Rebesco et al., 2014).

Small vertical offsets between reflectors of up to 0.005 s (~4 m) and columnar low-amplitude features occurring throughout all seismic profiles are attributed to small faults. They are found especially at Ridge RD1 (Figure 5) and around the Pontevedra Contourite.

While the deepest interpreted Horizon H0 is laterally not continuously resolved at the lower continental slope and inside GIB due to seismic signal penetration limits, six younger horizons
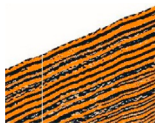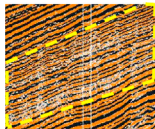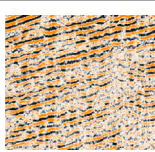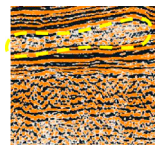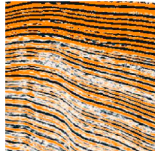
are identified and used to define seismic Units SU I to SU VI (Table 2).

H1 is the lowest unit boundary, separating **Seismic Unit I** (SU I) from the seismic basement. In wide areas it is conformable to reflectors below, however it onlaps on elevations of the base topography, e.g., the topographic obstacles (see OB1 in Figure 3). On the northern side of Ridge RD 1 it bounds reflector truncations. SU I generally is characterized as modified sheeted drifts. Facies B, with some patchy low amplitude areas, might result from intercalated MTDs below seismic resolution near Obstacle OB1 (Figure 3), on the northern flank of Ridge RD1 and in the Lower Slope Basin (Figure 4). It is mostly conformable to H1 except for its onlaps on the base topography.

H2 bounds SU I from **Seismic Unit II** (SU II). It is widely subparallel to the underlying SU I reflectors except for the areas at the canyons (Figure 4) where it downlaps on H1. On top of RD 1 it truncates SUI reflectors.

SU II mostly consists, similarly to Unit SU I, of sheeted drifts (Facies B) intercalated by a few patchy MTDs (Facies C1) as detectable underneath the Pontevedra Contourite and the Lower Slope Basin (Figure 4). A pronounced thickness variation in the Pontevedra Contourite overlies a slope angle change in H2. The steeper slope close to OB 1 is overlain by a thin part of SU II with a parallel reflector configuration. Where the slope is gentler (visible in the center of line GeoB11-019 in Figure 3) SU II becomes thicker, the internal reflectors

TABLE 1 Classification of seismic facies type used in this study with illustrative examples and interpretation.

| Type	Continuity	Amplitudes	Reflector spacing	Reflector geometry	Example	Interpretation
A1	Highly continuous	High	Large	Subparallel		High amplitude sheeted contourite drifts
A2	Highly continuous	Medium	Dense	Subparallel		Sheeted contourite drifts
B	Semi continuous	Low to medium	Medium to large	Subparallel to contorted		Altered sediments of different origin prevalently sheeted contourite drifts
C1	Discontinuous	Medium to transparent	Medium	Contorted to chaotic		Mass waste deposits with disturbed to no internal structure
C2	Discontinuous	High	Medium	Contorted to chaotic		Tectonically altered sediments, seismic basement
D	Highly to semi continuous	High to low	Dense to large	Divergent and convergent		Other contouritic drifts including plastered and mounded drifts

diverge (Facies D), and the upper boundary, H3, is slightly convex. Barring exceptions like this, H3 in general is subparallel to the underlying reflectors. Also at the canyons, similarly to H2 downlaps and on top of RD 1, it truncates underlying reflectors.

Seismic Unit III (SU III) overlies H3 and consists of sheeted contourite drifts (Facies B) and MTDs (Facies C1), comparable to Units SU II and SU I. High amplitudes on the crest of Ridge RD1 indicate coarse sediment (Figure 4). Near the Obstacle OB1 a mounded feature occurs (Figure 3). As the indicative (Facies D) is not clearly recognizable it is debatable whether this is a mounded or a plastered drift.

This mounded feature of course is imprinted in H4 as the upward boundary of SU III. H 4 is in most areas a conformable boundary. It is not present on the southern flank of RD 1 but above all canyons only crudely following the topography of H3. The **Seismic Unit IV** (SU IV) above H4 is generally characterized by a stratigraphic succession of medium-amplitude, sheeted contourite drifts (Facies A2) local reflector divergence (Facies D), and sheeted contourite drifts containing some MTDs (Facies B; Figures 3, 4). A vertical succession of several mounds is located near OB1, separated from the obstacle by local depressions within SU IV (Figure 3 close-

up). H5 as the upper boundary of SU IV is present in almost the entire area and conformable to underlying reflectors. The overlying **Seismic Unit V** (SU V) exists over vast areas in the form of high amplitude sheeted contourite drifts in its lower stratigraphic portion (Facies A1) and of sheeted drifts in the upper portion (Facies A2). MTDs occur in the Lower Slope Basin and inside the canyons (Figure 4). Similar to SU IV, mounded contourite drifts (Facies D) are present near topographic obstacles and on Ridge RD1, overlying the mounded Unit SU IV contourite drifts (Figures 3–5). Unit SU V does not onlap on the seismic basement at OB1 but is, instead, separated from this obstacle by a U-shaped, 2.5 km wide erosional channel, visible at the modern seafloor (Figure 3). H6 as the upper boundary of SU V is mainly conformable except for reflector truncations at a step in Horizon H6 west of the depocenter next to Obstacle OB1 (Figure 3) and at both sides of a through-shaped depression in H6 (Figure 4). **Seismic Unit VI** (SU VI) on top of H6 almost entirely consists of high amplitude sheeted contourite drifts (Facies A1) while Facies A2 (sheeted contourite drifts) only occurs sparsely. Some MTDs (Facies C1) are limited to the Lower Slope Basin (Figures 3, 4). Mounded contourite drifts (Facies D) concentrate just next to topographic obstacles and on RD1 (Figures
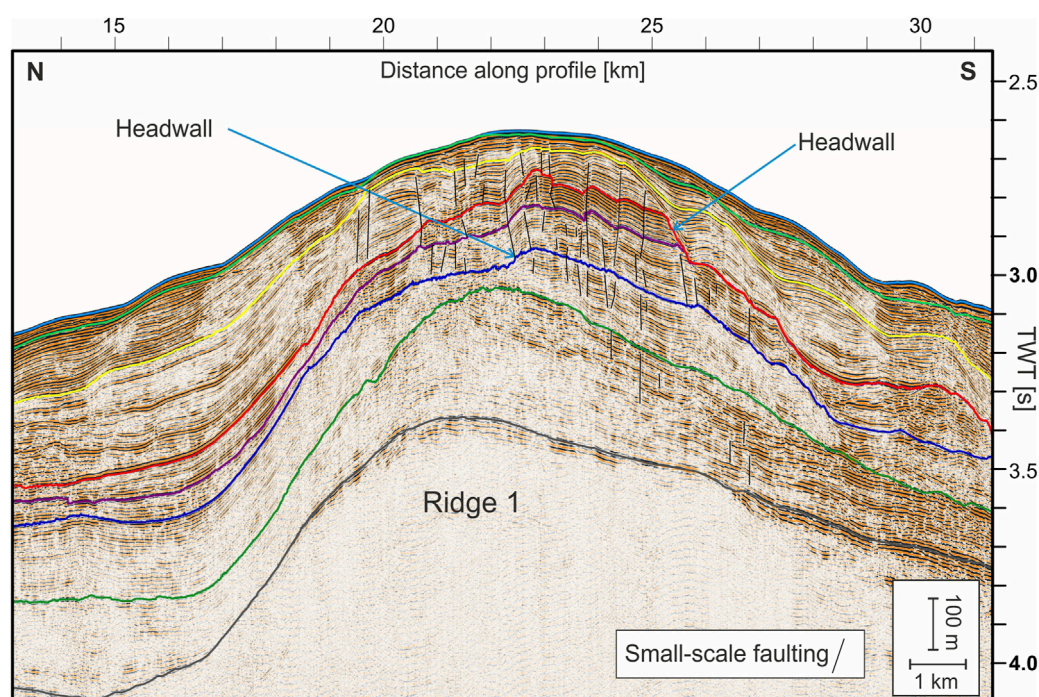
FIGURE 5
Close-up of seismic Profile GeoB11-010 around Ridge RD1, showing the sedimentary features on the ridge. Small scale faults and headwalls are indicated by lines. For the exact location of the close-up see Figure 4.

3, 4). Unit SU VI is separated from Obstacle OB1 by the same erosional channel, as was the case for Unit SU V (Figure 3). Interestingly, small wavy elements overlie the location where Unit SU V reflectors carve a morphological step into H6 (Figure 3).

4.3 Sediment thickness maps

Seismic basement and base topography: The buried surfaces of the topographic obstacles and the upper and middle slope are not of a sedimentary nature, but were interpreted as the top of a (seismic) basement, on which the overlying seismic Units SU I to SU IV onlap (Figures 3, 4). To create a base topography that covers the entire area of interest, the interpreted seismic basement was blended with Horizon H1. The resulting map (contour lines in Figure 6A) reveals a buried topography at a varying depth of 4.1 to 0.5 s TWT. This deep paleo-topography contains most of the same structural elements also found at the modern surface (Figure 2). Obstacles OB1 to OB4 are clearly visible as local heights with steep flanks, although the deeper part of OB3 extends further to the northwest than today, describing a hook-like shape, and OB4 incorporates a buried elongated depression (Figure 6A). The morphology of Ridge RD1 already had an expression in the Base Topography. Buried local depressions occur in the area of RD2, in contrast to the modern bathymetric situation, and underneath the modern Arosa Canyon. At the location of this canyon, the respective old depression is a product of erosional truncation of H1; similar truncations also occur at the northern flank of RD1 (Figure 4).

The thickness map of **Seismic Unit I** (SU I) (Figure 6A) reveals that the areas of maximum thickness reach up to 0.26 s TWT and are clearly attributed to former depressions in the underlying topography filled by sheeted drift deposits and MTDs. The spatially most widespread thickness maximum in the Lower Slope Basin stretches over at least 30 km in both N-S and E-W directions. At the Pontevedra Contourite, where the underlying topography is gently elevated, the thickness of Unit SU I is reduced to about 0.016 s TWT. The local depression underneath Ridge RD2, which spans about 10 km in diameter, hosts a 0.013 s TWT thick sediment infill. The small-scale depression, which is part of the complex Base Topography of Obstacle OB4, has a size of 5 km and is similarly filled by a depocenter.

The existence of depocenters directly north of Ridge RD1 is, in contrast, not steered by pre-existing confined topographic lows. Instead, the apparent extreme thickness on the ridge flank is an artefact of the steep topography (Figure 4). Unit SU I covers neither the major canyons nor the upper and middle slope or the topographic Obstacles OB1, OB2, and OB3; it also does not occur in an area northeast of OB3 and in the vicinity of the elevated areas of OB4. Lateral stratigraphic transitions towards zero thickness around topographic obstacles and at the middle slope are associated with onlapping reflections (Figures 3, 4). Contrarily, the lateral thickening from the Arosa Canyon towards the Pontevedra Contourite and between Canyon CY2 and Ridge RD1 (Figure 4) is accompanied by internal reflector divergence. Thickness variations from thin to medium thick (0.065–0.160 s) stratigraphic intervals occur at the canyon flanks and on top of RD1 due to reflector truncations at Horizon H2 (Figure 4).

Seismic Unit II (SU II) covers a wider area than the underlying Unit SU I. Maximum sediment thickness of up to 0.28 s TWT is

TABLE 2 Overview of interpreted horizons and seismic units.

Horizon	Seismic Unit	Seismic facies	Deposition style	Median Unit thickness (compaction corrected)
Seafloor				
	SU VI	A1, A2, C1, D	Filling up topographic lows, topography build-up, non-deposition on Ridge RD 1	59 m
H6				
	SU V	A1, A2, C1, D	Topography build-up, mass wasting, and filling up topographic lows	83 m
H5				
	SU IV	A2, B, C1, D	Topography build-up and filling of topographic lows	152 m
H4				
	SU III	B, D	Filling up topographic lows and building small, localized mounds	61 m
H3				
	SU II	B, C1, D	Filling up topographic lows and mass wasting, gentle topography build-up	63 m
H2				
	SU I	B	Filling up topographic lows	51 m
H1–Base topography				
	seismic basement	C2	–	–

found in depressions that are present along Horizon H2 between Obstacles OB3 and OB4, and west of OB3 (Figure 6B). Two depocenters in the Lower Slope Basin, each 10 km in diameter, reach a thickness of 0.26 s TWT. These depocenters correlate with depression in the underlying topography as well. Local thickness variations from medium thin to medium thick (0.1–0.2 s TWT) have developed on a scale of a few km at the Pontevedra Contourite and west of OB1. The character of deposits is determined by a small-scale topography of H2 combined with the existence of small MTDs (Figure 4) and the presence of a plastered contourite drift (Line GeoB11-019; Figure 3). A reduced unit thickness (0.1–0.15 s) is also found at canyon flanks and on top of RD1, where the strata indicate erosional reflector truncations (Figure 4). The canyons themselves, the middle to upper slope, and the topographic heights are not covered by Unit SU II. Their lateral transition towards zero thickness is associated with reflector onlaps.

The thickness distribution of **Seismic Unit III** (SU III) differs significantly from the two underlying units since the Lower Slope Basin and a major part of the Pontevedra Contourite are characterized by a lower than medium depositional thickness of 0.09–0.1 s TWT (Figure 6C). Thickness maxima within Unit SU III of up to 0.24 s TWT are found only in the form of small localized depocenters, rarely exceeding 5 km in diameter, around Obstacle OB1, on top of Ridge RD1, along the Arosa Canyon, and inside

Canyon CY2. Since the seaward portion of the depocenter near OB1 is obscured by very low amplitudes, reflector truncations in this area can only be inferred (Figure 3). Locally confined depocenters, up to 0.13 s TWT thick, also occur west of OB2 and OB4. Over most parts of the study area there is, however, no correlation between the thickness of Unit SU III and underlying topographic elements. Only local depressions that pre-existed inside the canyons are filled with SU III deposits. The seismic data reveals an absence of SU III on the southern flank of Ridge RD1 by reflector truncation at Horizon H4 (Figures 4, 5). The topographic obstacles and the middle and upper slope are bare of Unit SU III, though the uncovered areas are smaller in their lateral extent when compared to SU II. Limited areas without SU III (<5 km in size) also occur at the southern flank of Ridge RD1.

Seismic Unit IV (SU IV) generally displays a continuous thickness across major parts of the study area (Figure 7A) and, with its maximum sediment thickness of 0.4 s TWT, is considerably thicker than the underlying seismic units (Figure 7A). Several local thickness maxima occur within the depression of the Arosa Canyon. Another maximum is related to the H4 topography in the southern part of the Pontevedra Contourite (Figure 3; Figure 7A). The thickness of Unit SU IV varies between 0.2 and 0.3 s TWT in the remaining area of the Pontevedra Contourite, the Lower Slope Basin, and directly north of Ridge RD1.
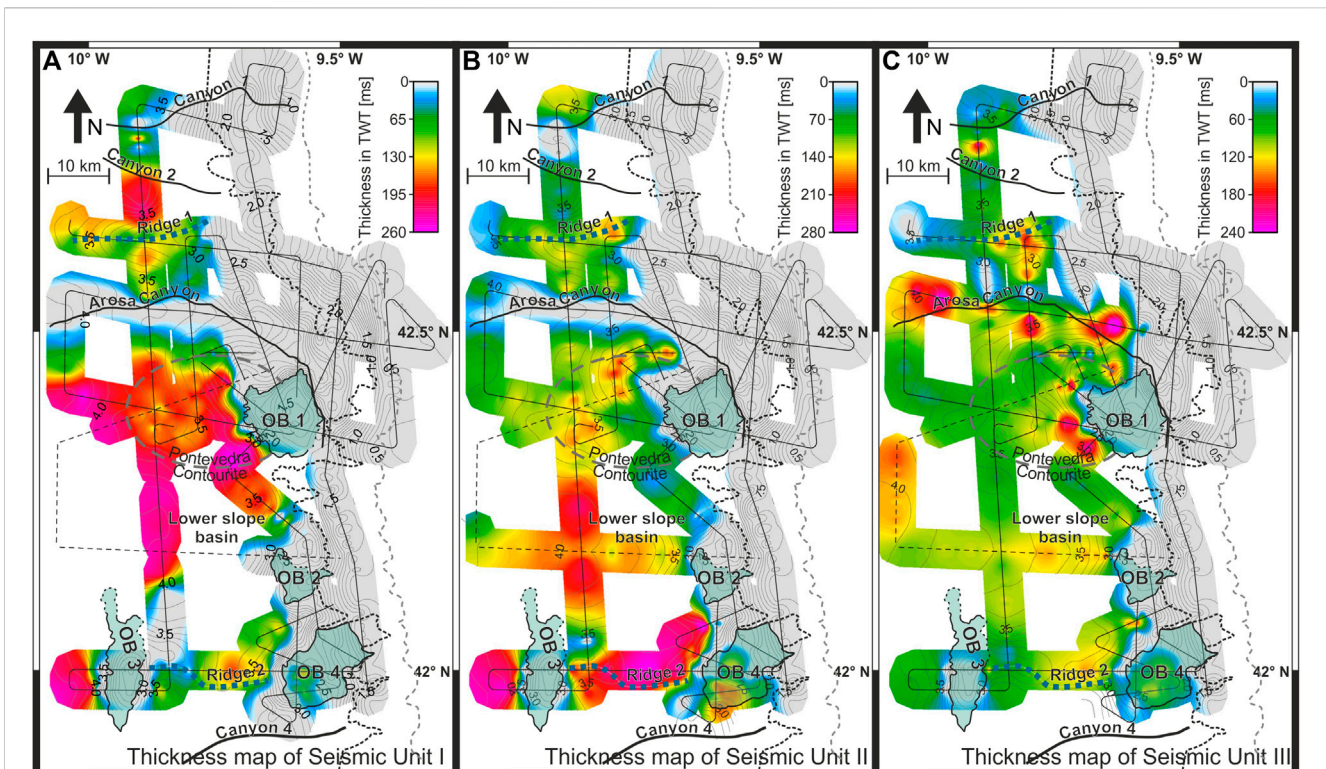
FIGURE 6
Thickness maps of Seismic Units SU I, SU II, and SU III. Contour lines represent the respective underlying topography **(A)**: SUI and reflection Horizon HR1 **(B)**: SU II and HR2, **(C)**: SU III and HR3). For a better geographic orientation, the main features from the interpreted bathymetry are overlain (see Figure 2B). The dashed grey and black lines indicate the transition from upper to middle and from middle to lower continental slope, respectively.

Thickness variations on a scale of a few kilometers in width are associated with MTDs as well as local depressions in Horizon H4 (Figure 4). The contour lines of H4 distinctively show that Ridge RD2 exists as a topographic feature at this time (Figure 7A). The thickness distribution on Ridge RD1 is patchy and partly reduced to zero due to reflector truncations (Figures 4, 5). Another small SU IV-free patch of less than 3 km in diameter is located northwest of Obstacle OB1. Also, the topographic obstacles and the middle and upper slope are not covered by Unit SU IV. Compared to SU III, the overall extent of uncovered areas is smaller, though.

In the Pontevedra Contourite and the Lower Slope Basin, up to nine successive sub-units can be distinguished within SU IV, while six of these sub-units occur on Ridge RD1. The thickness of sub-units within the sheeted drifts varies from 0.01 to 0.1 s TWT. Mounded drifts are particularly present in proximity of topographic obstacles, on RD1, and above the irregular topography in Horizon H4 (Figures 3–5).

In **Seismic Unit V** (SU V) some thickness maxima are associated with pre-existing depressions in H5 as well as with Canyons CY1 to CY3 and the gully north of Obstacle OB4 (Figure 7B). They reach up to 0.22 s TWT and extend over 10–15 km. Other maxima that do not correlate with H5 topography occur west and north of OB2 and west of OB1 separated by an erosional channel (e.g., Figure 3). Overall, the Lower Slope Basin, the Pontevedra Contourite, and the area north of Ridge RD1 host higher sediment thickness (0.12–0.14 s TWT). Where Unit SU V overlies RD1, the unit is less than 0.06 s TWT thick and partly absent. An area of about 3 km northwest of Obstacle OB1 as well as OB1 to OB3 and parts of OB4 are bare of Unit SU V.

The main thickness maxima of **Seismic Unit VI** (SU VI), located on the Pontevedra Contourite, inside the Lower Slope Basin and a gully north of Obstacle OB4 are associated with depressions in Horizon H6 (Figure 7C). The depocenters inside the gully and north of OB4, here not related to H6 topography, reach exceptional thicknesses of 0.18 s TWT; the other two maxima are not thicker than 0.13 s TWT.

The thickness distribution of Unit SU VI is very patchy in the northern part of the study area, varying from 0 to 0.18 s TWT over distances of less than 2 km. Several of these minimal patches align with the Arosa Canyon depression (Figure 7C) where the internal reflectors truncate at the canyon flanks (Figure 4). SU VI strata on the Ridge RD1 crest are less than 0.02 s TWT thick with a patchy distribution. It is, furthermore, noteworthy that Obstacle OB4 is covered by elongated SU VI sediment patches that show a N-S orientation, are approximately 2 km wide, and vary in thickness between very thin (0–0.02 s TWT) and medium thick (0.05–0.09 s TWT); the easternmost patch of those reaches an exceptional thickness of 0.18 s TWT. Unit SU VI does not exist at OB1 to OB3 and in the southern region along the middle and upper slope, though two very thin (0.02 s TWT) spots, smaller than <2 km, occur northwest of OB1.

5 Discussion

To discuss the stratigraphic history and palaeoceanographic evolution of the Galicia Continental Margin, depositional and erosional processes and products are correlated with both changes
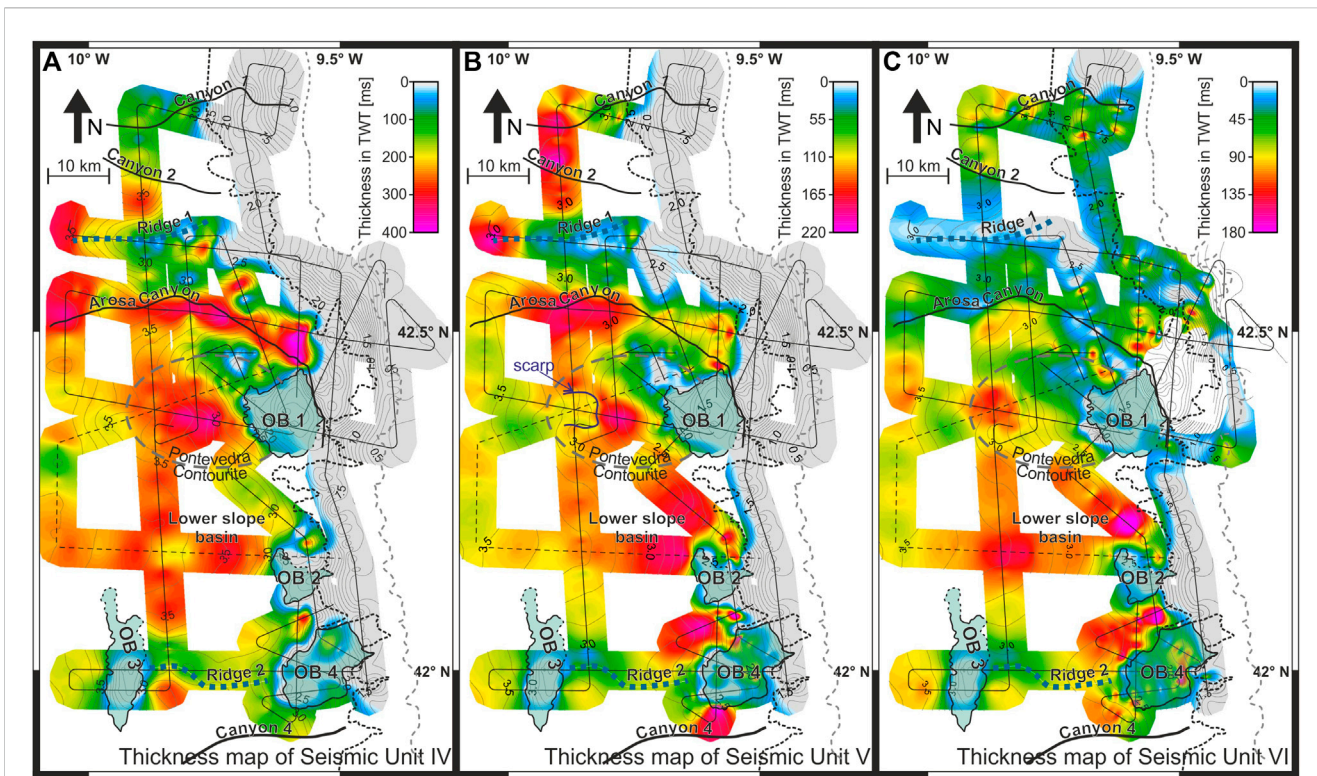
FIGURE 7
Thickness maps of seismic Units SU IV, SU V, and SU VI. Contour lines represent the respective underlying topography **(A)**: SU IV and HR4 **(B)**: SU V and HR5, **(C)**: SU VI and HR6. For a better geographic orientation, the main features from the interpreted bathymetry are overlain (see Figure 2B). The dashed grey and black lines indicate the transition from upper to middle and from middle to lower slope, respectively.

in large-scale palaeoceanographic conditions within the North Atlantic Ocean basin and regional tectonics. The aim is to a) establish a solid stratigraphic model and b) reconstruct the specific impacts the various external forces had on margin sedimentation and stratigraphy.

5.1 Pre-mid-Eocene deposition shaping the base topography

The stratigraphic Horizons H0 and H1 were dated to 89.9 Ma (Coniacian-Santonian boundary/Upper Cretaceous) and 41 Ma (Lutetian-Bartonian boundary/mid-Eocene), respectively, by a correlation with seismic data from Murillas et al. (1990). The deposits in-between these two stratigraphic boundaries are identified as a hemipelagic, post-rift sequence and found inside GIB as well as on the Galicia Bank (Murillas et al., 1990; Ercilla et al., 2008).

Neighboring drift systems from the Cretaceous have formed in greater water depths than the study area. At the deeper Iberian Margin South and West of the study area, contourite drifts as well as widespread erosion show the effect of Tethyan outflow through the strait of Gibraltar (Soares et al., 2014). The widespread hemipelagic deposition in the working area could be for two reasons: a) these currents did not penetrate sufficiently into the GIB or b) the current had already ceased at the formation of H0 89.9 Ma. Another pathway for vigorous Tethyan outflow was the Pyrenean corridor which was recorded in contouritic drifts in the Bay of Biscay northeast of the study area (Liu et al., 2023). Following Coriolis,

veering this branch of Tethys outflow would have flown northward and thus never reached the Iberian margin.

In a global oceanographic context, the Upper Cretaceous to early Eocene hemipelagic succession has accumulated when the Indian Ocean–Mediterranean Seaway (western Tethys Ocean remnants) and the Central American Seaway (CAS) were still fully functional serving as bottleneck passages for the Mesozoic-style circum-equatorial ocean circulation (Montes et al., 2015; Straume et al., 2020; Torfstein and Steinberg, 2020). Also, the Central Atlantic Gateway had opened and deepened, providing a full oceanographic connection between North and South Atlantic Ocean basins (Batenburg et al., 2018; Dutkiewicz and Mueller, 2022). However, AMOC as the main engine for the modern-style N-S directed deep-water circulation dynamics was not established before mid-Eocene due to the absence of a Norwegian-Greenland Seaway that would allow for high-latitude deep-water formation (Miller et al., 2009; Abelson and Erez, 2017; Coxall et al., 2018; Hovikoski et al., 2021). In the absence of a significant AMOC driving open-ocean geostrophic currents, hemipelagic sedimentation has prevailed in the study area in the GIB as well.

5.2 Basin morphology in the mid-Eocene (41 Ma)

The mid-Eocene Base Topography (Horizon H1; 41 Ma) represents the termination of this ancient sedimentary regime.

This paleo-surface also bounds those areas that were bare of deposition before, including the topographic Obstacles OB1 to OB4, Ridge RD1, as well as the steep middle slope. The correlation with the main tectonic elements mapped by Murillas et al. (1990) reveals that RD1 is related to a structural anticline (Figure 2B). Obstacles OB2 to OB4 are linked to an N-S trending horst and graben system in the south part of the study area, which presumably evolved during the rifting and opening phases of GIB in early Cretaceous times (Murillas et al., 1990; Vázquez et al., 2008). RD1 and OB1 experienced further uplift during the Pyrenean Orogeny in the mid-Eocene (Murillas et al., 1990). Reflector truncations at H1 on the crest of Ridge RD1 are interpreted as scarps caused by successive sediment mass failure events (Figure 4), which were probably triggered by an over-steepening of the slope in the run of the mid-Eocene uplift. The modern canyons are not related to such long-lived tectonic features, and Canyon CY3 was the only conduit that cut into the Eocene Basin Topography. While this paleo-canyon did not erode into the late Cretaceous succession of Horizon H0, suggesting an age not older than 89 Ma for its initial formation, Canyons CY1 and CY2 did not even reach down to the Base Topography (Figure 4), indicating that they are much younger.

The Base Topography representing the basin morphology dated to 41 Ma corresponds to a global circulation setting prior to the opening of a deep-water Drake Passage. An open Tethys and open Central American seaway allowed for a circum-equatorial circulation. Deepwater was prevalently created in the southern high latitudes and flowed northward through the Central Atlantic which was open since 59 Ma (Selandian-Thanetian boundary/mid- to late Paleocene; (Dutkiewicz and Mueller, 2022)).

5.3 Initial contouritic deposition and downslope transport in the mid-to late Eocene (41–35 Ma)

Unit SU I rests on the Base Topography and began to form in mid-Eocene times. The location of major depocenters in the deep and low-gradient area of the Lower Slope Basin (Figure 6A) together with the occurrence of sheeted contourite drifts and MTDs (Figures 3, 4) suggests that both gravity-driven downslope and contour current-driven along-slope sediment transport co-existed. Both processes led to a levelling of the pre-topography by sediment accumulation inside depressions, mainly the Lower Slope Basin (Figure 6A). No depositional fill is found inside Canyons CY1, CY2, and CY3 for the Eocene time interval, which might be due to the coinciding development of these conduits; while they have been highly active and cutting down at this time, large amounts of material that mainly bypassed the area in the form of mass flows from the middle and upper slope have provided the material found in Unit SU I deposits within the deeper GIB. These successions point to Eocene tectonic activity (Le Pichon and Sibuet, 1971; Vázquez et al., 2008) that, in turn, triggered those mass wasting events.

Additionally, sediment downslope creeping occurred particularly on top of Ridge RD1 and, to a lesser extent, at the Pontevedra Contourite, as evidenced by a series of small faults (Figures 3–5). These faults do not extend into the underlying strata characterizing them as early-post-depositional and not tectonic origin. This slope creeping is interpreted as a consequence of Ridge RD1 and Obstacle

OB1 uplift during the Pyrenean Orogeny (Murillas et al., 1990). The uplift dynamics also caused true slope failures as indicated by headwall scarps on top of RD1 (Figures 4, 5). The overall patchiness in depositional thickness at this ridge can, therefore, be attributed to the presence of erosional scarps at higher ridge elevations and the presence of MTDs at its southern lower flank.

Furthermore, a convex-shaped contourite drift occurs in the area of the Pontevedra Contourite, which thins out in the northern direction towards the Arosa Canyon (Figure 4). This thinning might be the remnant product of erosion, resuspension, and westward contouritic transport of sediment that was originally contributed to by turbidity currents (cp. Bender et al., 2012; Hanebuth et al., 2015). Although the drift body does not constitute a characteristic thickness maximum, the topography-smoothing redistribution of sediment clearly points to an impact of bottom currents on Unit SU I deposition. The lack of well-defined contouritic depocenters in Unit SU I suggests, however, that the bottom-current velocity was relatively subtle, as the type of sheeted contourite drifts forms under weak to moderate bottom currents of less than 5 cm/s (Faugères et al., 1999; Stow et al., 2008; 2009).

The origin of these minor bottom currents can not be deciphered unambiguously. Since a contribution of neither NCW nor significant Tethys Outflow Water to the North Atlantic Ocean circulation seems to be probable for this timeframe (Thomas et al., 2003; Scher and Martin, 2008; Straume et al., 2020); the main source of bottom water was probably located in the South Atlantic (Miller et al., 2009). Contouritic drifts near the Madeira Islands grew under the influence of SCW at this time frame (Roque et al., 2023), showing that there was still considerable northward transport of southern sourced bottom waters. Overall, the Eocene South Atlantic shows little indication for an AMOC (Uenzelmann-Neben et al., 2017). These findings underline the assumption that Atlantic Ocean circulation did not significantly change during the Eocene (Poore et al., 2006).

The transformation from an earlier hemipelagic regime towards a slowly incipient bottom-current influenced situation seems to reflect the global tectonic evolution. The Central Atlantic Gateway had been fully opened by 59 Ma (Selandian-Thanetian boundary/mid-to late Paleocene; Dutkiewicz and Mueller, 2022), and the Norwegian-Greenland Seaway was successively widening and deepening between 40 and 34 Ma (Bartonian to the Priabonian-Rupelian boundary/mid-to late Eocene; Poore et al., 2006; Straume et al., 2020), initiating significant NCW formation that spread out over the two Atlantic Basins in the eastern North Atlantic Ocean basin (Langton et al., 2016; Via and Thomas, 2016; Hovikoski et al., 2021), while the circum-equatorial water exchange was still ongoing (Hernández-Molina et al., 2022). The increasing intra-basinal, inter-polar meridional water exchange, as well as the early and successively intensifying AMOC-controlled North Atlantic deep-water formation, had, thus, started to influence the margin sedimentation pattern, in addition to the regional to local tectonic stress impact.

5.4 MTD and contourite deposition from late Eocene to mid-Miocene (35–14 Ma)

Unit SU II mainly accumulated inside the Lower Slope Basin and in local depressions within the HD2 paleo-topography. As the

most marked difference to Unit SU I, the geometry of the contourite drift next to Obstacle OB1 transformed from a formerly sheeted (widely extended), into a plastered (slope-connected) contourite drift, which built up at water depths greater than 3.4 s TWT (ca. 2,550 m; Figure 3). A reasonable explanation for this change in drift geometry is the establishment of a new water-mass boundary. The Norwegian-Greenland Seaway opening between 40 and 34 Ma led to an onset and successive intensification of NCW overflow and discharge through the Faeroe-Shetland Channel (Davies et al., 2001; Poore et al., 2006; Hovikoski et al., 2021). NCW has been present throughout the whole Atlantic Basin since early Oligocene times (Via and Thomas, 2006), though it was probably less dense and, thus, shallower than today (Knutz, 2008). NCW can be considered a suitable candidate for establishing such a new water-mass boundary inside GIB by overlying the currently basin-wide present southern-sourced deep water.

The plastered contourite drift does not appear as a distinct depocenter in the thickness map (Figure 6B). Instead, the small-sized thickness maxima within the Pontevedra Contourite are intercalated by MTDs (Figure 4), indicating that downslope processes gained dominance over the general sedimentation pattern. The greatest thickness of SU II occurs within the depression, which underlies Ridge RD2. Most likely, the mid-slope gullies provided sufficient sediment to fill this topographic low, with Obstacle OB3 acting as a barrier for near-bottom sediment transport to expand further basinwards. As a result, the associated depression below Ridge RD2 had filled up and an initial ridge topography formed (H3 contour lines in Figure 6C). MTDs occur in the Lower Slope Basin and on the Pontevedra Contourite, while faulting can be identified at Ridge RD1 and the Pontevedra Contourite, similar to the situation during the SU I time interval. There are, in addition, no deposits preserved inside any of the canyons, and the sediment thickness distribution on RD1 is still of a patchy nature, again coinciding with several slope scarps (Figure 4). All these observations suggest that down-slope sediment transport became a dominant mechanism from late Eocene until mid-Miocene, probably triggered by tectonic activity of the ongoing Pyrenean Orogeny (Vázquez et al., 2008; Martín-González and Heredia, 2011).

5.5 Onset of separated mounded drifts and MTD deposition in mid-Miocene to early Pliocene (14−4.5 Ma)

The most profound change in sedimentation pattern between Unit SU II and **Unit SU III** is that the major depocenter migrated from the Lower Slope Basin into the vicinity of Obstacle OB1 and into the Arosa Canyon (Figure 6C). Deposition maxima of 5–10 km in size are concentrated in specific local areas, as was observed for the preceding units SU I and SU II. In SU III this is due to the occurrence of small MTDs inside the canyon and around the Pondevedra Outlier (Obstacle OB1), and also the build-up of mounded contourite drifts (Figure 3). The existence of MTDs and scarps, which are also found on Ridge R1, in concert with a significant number of faults, points to a succession of slope failures and thereby yet ongoing tectonic activity. However, the first appearance of mounded contourite drifts separated by a moat from

OB1 provides evidence for an increasing impact of contour currents on sedimentation. In Unit SU III, the relief of the moat is not very pronounced and deposition of sediments within the moat classify it as a constructional moat (Wilckens et al., 2023a). Flume tank experiments imply that, taking the morphology into account, the bottom current speed must have exceeded 10 cm/s to form such a moat (Wilckens et al., 2023b). Additionally, the formation of a moat suggests that the bottom current has been particularly focused against the slope due to Coriolis veering (Faugères and Stow, 2008; Rebesco et al., 2014). To achieve this slope-leaning current, a distinctly northward-directed bottom flow is required. This change of sedimentation pattern was, thus, likely linked to the reorganization of the Atlantic and global ocean circulation pattern, which included the establishment of the circum-Antarctic current system and the closure of the Tethyan-Indian connection terminating the circum-equatorial flow at 14 Ma (Stille et al., 1996; Rögl, 1999; Straume et al., 2020; Torfstein and Steinberg, 2020; Dutkiewicz and Müller, 2022). The semi-enclosed Tethys Ocean already resembled the Mediterranean Sea at this stage (Scher and Martin, 2008; Hernández-Molina et al., 2022); a general ocean circulation pattern providing an effective exchange with the Atlantic Ocean similar to modern conditions is, thus, to be expected. Indications for Atlantic surface water inflow and intermediate Tethys water outflow were described for, at least, late Miocene times (14 Ma; Kouwenhoven and van der Zwaan, 2006). Since the mounded contourite drifts are attributed to such a Tethys outflow, the boundary between Units SU II and SU III can be dated to 14 Ma. The MTDs were presumably triggered during the Betic Orogeny by the uplift of the Beiral de Viena Block, which underlies the southern part of the study area (Figure 1A; Muñoz et al., 2003).

During the Miocene, the subsidence of the Iceland-Faeroe Ridge opened a new pathway for NCW to contribute to the North Atlantic bottom water formation (Stille et al., 1996; Straume et al., 2020). By 14 to 12 Ma, the prevalent bottom-water flow reversed into a southward-direction (Woodruff and Savin, 1989), a situation similar to the modern Atlantic Meridional Overturning circulation system. Shoaling of the Central American Seaway (CAS) 12 to 10 Ma ago restrained a Pacific-Atlantic exchange at low latitudes to 1,000 water depth (Duque-Caro, 1990 Montes et al., 2015; Karas et al., 2017), which further aided a southward transport of NCW (Nisancioglu et al., 2003; Preu et al., 2012) and strenghtend the AMOC (Alves et al., 2023). None of these major oceanographic changes, however, left a distinct enough imprint on the deposits at the Galicia Continental Margin to be detected in the high-resolution seismic data.

5.6 Major contourite drift built-up from the early Pliocene to early Pleistocene (4.5−2.4 Ma)

During the time **Unit SU IV** has evolved, contouritic activity was more frequent and its control on sediment thickness more effective than was the case for the antecedent units. Also, sedimentation rates rose substantially (Figure 8), implying that significantly larger amounts of sediment were supplied to the Galicia continental margin. The Lower Slope Basin is covered by sheeted contourite drifts of 0.25 s (190 m) thickness. Minor variations in thickness are
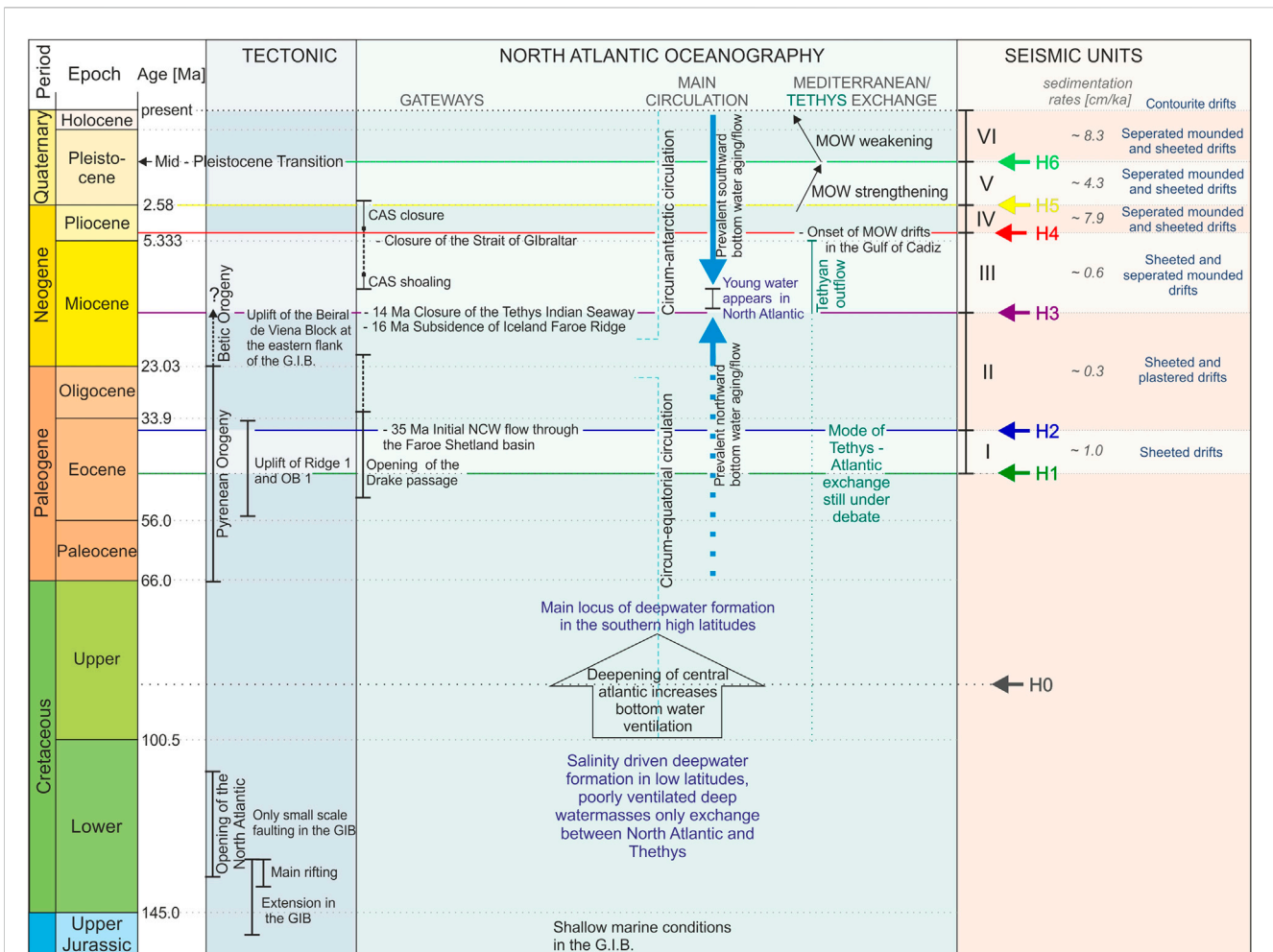
FIGURE 8
Timeline of the evolution of the Galicia continental margin, summarizing the tectonic evolution of the North Atlantic Ocean basin and GIB (Boillot et al., 1979; Murillas et al., 1990; Muñoz et al., 2003), the oceanographic evolution of the North Atlantic Ocean basin (Roth, 1986; Woodruff and Savin, 1989; Duque-Caro, 1990; Stille et al., 1996; Haug and Tiedemann, 1998; Rögl, 1999; Davies et al., 2001; Nisancioglu et al., 2003; Via and Thomas, 2006; Robinson and Vance, 2012; Hernández-Molina et al., 2014; Bell et al., 2015), and the findings from this study.

attributed to either mass-wasting deposits or filled local depressions. Main thickness maxima represent the infill of the Arosa Canyon. A fully separated mounded contourite drift developed in vicinity to the Pontevedra Outlier (Obstacle OB1; Figure 3). The moat geometry changes throughout SU IV (cp. close-up in Figure 3). Initially a high relief exists which is almost levelled by the end of the deposition of SU IV. Overall, the moat is constructional which, in combination with the leveling of the relief, hints at still moderate current speeds (Wilckens et al., 2023a). As a further effect of such an emerging current-topography interaction, the area at the lee (northward) side of Obstacle OB1 was characterized by non-deposition. Locally higher bottom-current velocities, preventing deposition, are attributed to eddy shedding as a consequence of the interaction between bottom current and OB1 (Boyer and Zhang, 1990; Hernández-Molina et al., 2006; Zhang et al., 2016b). Over the rugged topography of Ridge RD1, a wavy sediment pattern developed during deposition of Unit SU IV (Figures 4, 5). The patchy sediment distribution on top of RD1 may be credited to scarps and MTDs originating from the precedent Unit SU III. The

resulting pronounced topography of the SU III surface led to a modulation of the bottom-current regime during the subsequent deposition of SU IV.

The above-described interaction of bottom currents with the seabed topography is indicative of a vigorous, northward-flowing water mass. The flow direction is indicated through the position of the contourite and moat west of the Pontevedra outlier Outlier (Obstacle OB1; Figure 3) as well as eddy shedding north of it. Northward-flowing MOW is the prime candidate regarding the appropriate water depth to interact with the middle slope and topographic obstacles at the Galicia Continental Margin. MOW was established after the reopening of the Strait of Gibraltar (5.8–5.3 Ma; Hernández-Molina et al., 2011; Hernández-Molina et al., 2014). Over the past 4.5 Ma, the MOW velocity was strong enough to build up massive sand-prone contourite drifts inside the Gulf of Cadiz (Hernández-Molina et al., 2014). This initiation coincides with the build-up of Unit SU IV along the Galicia margin. Since the ultimate closure of the Central American Seaway from 4.2 to 2.4 Ma or 2.8 Ma (Newkirk and Martin, 2009; O'Dea et al., 2016; Karas et al., 2017), AMOC further intensified and

LSW reached the eastern North Atlantic Ocean for the first time (Nisancioglu et al., 2003; Bartoli et al., 2005). Hanebuth et al. (2015) identified ocean density fronts that migrated along the MOW–LSW transition zone during deglacial/early Holocene times as the major driving force for significant contourite drift build-up. It can, thus, be assumed that these density fronts are present and interact with the Galicia margin topography since both MOW and LSW have emerged in the study area.

5.7 Deposition from the early Pleistocene to Mid-Pleistocene Transition (2.4−0.7 Ma)

The deposition of **Unit SU V** took place under an enhancing bottom-current regime. The deep Lower Slope Basin does not host a distinct SU V depocenter but shows accumulation rates only slightly higher than medium thickness of sediments around 0.12 s (90 m), modulated by the H5 paleo-topography and MTDs (Figure 7B). Spatially extended thickness maxima are found over the Canyons CY 1 to CY3 (Figure 4). Wavy reflectors on the flanks of Ridge RD1 in combination with an extremely thin and patchy sediment distribution on its crest (Figure 5) indicate that the bottom-current accelerated during overflowing RD1, thereby leading to winnowing effects on the seabed. Further depocenters are situated around the Obstacles OB1, OB2, and OB4 and associated with separated mounded contourite drifts. Around the Pontevedra Contourite (Figure 3), the moat became erosional and the relief of moat and adjacent drift was enhanced, which is interpreted to be an effect of faster bottom currents including the development of secondary flows (Wilckens et al., 2023a; b). The moat remained since erosion and was active until modern times. A scarp located on the westward side of the contourite flank indicates failure dynamics of contouritic deposits (Figure 3; Figure 7B). A comparison between Units SU V and SU IV suggests that the hydrodynamic pattern of the bottom-current regime in interaction with the pre-existing topography was persistent; only the velocity had further intensified, leading to more pronounced depositional and erosional stratigraphic expressions. Overall seismic amplitudes, for instance, appear stronger, which can be attributed to the deposition of coarser material. A reduced sedimentation rate compared to the antecedent Unit SU IV suggests either increased sediment bypassing or temporary winnowing of already deposited sediments. Hernández-Molina et al. (2014) reported a MOW strengthening in the Gulf of Cadiz during the lower Pleistocene, which can be expected to have an effect along the entire MOW flow path along the Galicia margin. Nonetheless, the occurrence of coarser material might alternatively be attributed to a regional increase in coarser sediment supply, since global cooling and the onset of Northern Hemisphere Glaciations about 3 to 2 Ma ago (Raymo et al., 1992) might have favored continental erosion and a more direct terrigenous material supply to the ocean due to lower sea levels.

5.8 Along and across slope deposition from the Mid-Pleistocene Transition−Modern (0.7−0 Ma)

The thickness distribution of the youngest **Unit SU VI** is most variable, while sedimentation rates are highest compared to all older units (Figure 8). The most widespread depocenter in the Lower Slope Basin is associated with two mass-wasting deposits and the fill of a H6 depression (Figure 4). Two further thickness maxima are located north of Obstacles OB2 and between OB4 and OB2. Whilst the first maximum builds a positive local topography interpreted as a patch drift located at the lee side of the Pontevedra Outlier (Obstacle OB1; Figure 1A; Hanebuth et al., 2015), the second fills a depression connected to a slope gully (Petrovic et al., 2019). The observation exemplarily illustrates how various types of sediment-dynamics may occur under such hydro- and topographic conditions at a local scale. The crest of the separated mounded contourite drift associated with the Pontevedra Contourite migrates seaward, i.e., away from the obstacle, during the accumulation of Unit SU VI (Figure 3). However, the overall maximum thickness of the Pontevedra Contourite is not primarily related to the overall contourite drift geometry itself. It is, rather, caused by enhanced deposition inside the depression that is represented by the scarp in Horizon H6.

The wavy reflector pattern overlying the scarp, the existence of an area of non-deposition north of Obstacle OB1, which is attributed to eddy shedding, and the extremely reduced sediment thickness on Ridge RD1 (Figure 7C) associated with more wavy reflectors (Figures 4, 5) provide further evidence for lasting and intense bottom-current activity. Canyons CY1 to CY3, which had been completely filled during the SU V era, once again became reactivated and began to erode into Unit SU VI, as indicated by reflector truncations and sediment thickness minima.

In summary, a resumption of canyon activity, higher spatial depositional and erosional variability, and overall higher seismic amplitudes describe the main difference between the oceanographic Units SU VI and SU V. The boundary between these two units is associated with the climatic MPT (1.2–0.7 Ma) when a 40-kyr glacial-interglacial frequency transformed into 100-kyr cycles (Willeit et al., 2019). This global oceanographic change has similarly been documented in the Le Danois contouritic depositional system at the northern Iberian continental margin (Van Rooij et al., 2010). The Gulf of Cadiz contourite system further south shows a relative weakening trend in MOW intensity since the MPT (Hernández-Molina et al., 2014). These general changes in the depositional regime can, thus, be attributed to a regional weakening of the bottom-current conditions. The absence of tectonic faults, in contrast, indicates that slope failures and MTDs are not triggered by tectonic activity. The sedimentation rates on the slope and inside the GIB had drastically increased by a factor of four during high glacial times, a scenario which was attributed to the fluvial supply closer to the shelf break during the sea-level low stand intervals (Bender et al., 2012; Hanebuth et al., 2015), possibly supported by an associated slope oversteepening and turbidity current activity.

6 Conclusion

The high resolution multichannel seismic dataset at the Galician margin covers 41 Ma in total and facilitates a first-time analysis of the interaction between continental margin topography and oceanographic regime prior to Pliocene times. Six seismic units are identified and mapped, which reflect the evolution and interaction of across- and along-slope processes controlled by the

North Atlantic Ocean circulation. Since data for an exact age determination of these units is not available (i.e., by drilling), their age control relies on correlation tied with seismic data from Murillas et al. (1990) and especially on the careful linkage to changes in the oceanographic system. This analysis gives clear evidence that changes in the North Atlantic circulation caused by the open and closure of pathways far away have a distinct impact on the Galician margin sedimentary system. The stratigraphic evolution of the study area can be separated into six stages based on different interactions of bottom current with the topography.

- 41–35 Ma: Faint background currents smoothed topography and filled depressions. No specific current-topography interaction was observed.
- 35–14 Ma: Slight current strengthening led to the first interaction with topography creating plastered drifts, as a result of the onset of NCW production.
- 14–4.5 Ma: Development of initial separated mounded drifts related to Tethyan outflow water.
- 4.5–2.58 Ma: Establishment of quasi recent oceanographic conditions. Separated mounded drifts around topographic obstacles are fully developed and related to an interaction of MOW and LSW.
- 2.58–0.7 Ma: MOW strengthening and further drift build-up.
- 0.7 Ma–present-day: MOW weakening

During the build-up of the first three seismic units from Eocene to Pliocene, the Pyrenean and Betic orogenic activity led to faulting and triggered mass wasting. The increasing interaction between bottom current and topography reflects the evolution of North Atlantic Ocean circulation but was never able to fully level out the pre-existing morphology designed by tectonic processes. As soon as MOW started to impact the study area in the Pliocene, it has dominated the sedimentation pattern until today. Both reduced tectonic activity and enhanced continental sediment supply aid the more pronounced build-up of contouritic drift depocenters. Since the Mid-Pleistocene-Transition, the amount of slope failures and downslope sediment transport increase due to enhanced material supply from the hinterland.

In summary, this study exemplified in detail how the evolution of a passive continental margin is controlled by both basin wide oceanography and regional tectonics. It thereby provides a valuable showcase on how changes in the basin-wide circulation of the North Atlantic Ocean are recorded in small-scale regional sediment deposits.

Data availability statement

The raw data supporting the conclusion of this article will be made available by the authors, without undue reservation.

References

Conflict of interest

The authors declare that the research was conducted in the absence of any commercial or financial relationships that could be construed as a potential conflict of interest.

Publisher's note

Abelson, M., and Erez, J. (2017). The onset of modern-like Atlantic meridional overturning circulation at the Eocene-Oligocene transition: evidence, causes, and possible implications for global cooling. *Geochem. Geophys. Geosystems* 18, 2177–2199. doi:10.1002/2017GC006826

Alves, D. P. V., Maselli, V., Iacopini, D., Viana, A. R., and Jovane, L. (2023). Oceanographic exchanges between the Southern and Northern Atlantic during the Cenozoic inferred from mixed contourite-turbidite systems in the Brazilian equatorial margin. *Mar. Geol.* 456, 106975. doi:10.1016/j.margeo.2022.106975

Bartoli, G., Sarnthein, M., Weinelt, M., Erlenkeuser, H., Garbe-Schönberg, D., and Lea, D. W. (2005). Final closure of Panama and the onset of northern hemisphere glaciation. *Earth Planet. Sci. Lett.* 237, 33–44. doi:10.1016/j.epsl.2005.06.020

Batenburg, S. J., Voigt, S., Friedrich, O., Osborne, A. H., Bornemann, A., Klein, T., et al. (2018). Major intensification of Atlantic overturning circulation at the onset of Paleogene greenhouse warmth. *Nat. Commun.* 9, 4954. doi:10.1038/s41467-018-07457-7

Bell, D. B., Jung, S. J. A., Kroon, D., Hodell, D. A., Lourens, L. J., and Raymo, M. E. (2015). Atlantic deep-water response to the early Pliocene shoaling of the Central American Seaway. *Sci. Rep.* 5, 12252. doi:10.1038/srep12252

Bender, V. B., Hanebuth, T. J. J., Mena, A., Baumann, K.-H., Francés, G., and von Dobeneck, T. (2012). Control of sediment supply, palaeoceanography and morphology on late Quaternary sediment dynamics at the Galician continental slope. *Geo-Marine Lett.* 32, 313–335. doi:10.1007/s00367-012-0282-2

Blake-Mizen, K., Hatfield, R. G., Stoner, J. S., Carlson, A. E., Xuan, C., Walczak, M., et al. (2019). Southern Greenland glaciation and Western Boundary Undercurrent evolution recorded on Eirik drift during the late Pliocene intensification of northern hemisphere glaciation. *Quat. Sci. Rev.* 209, 40–51. doi:10.1016/j.quascirev.2019.01.015

Boillot, G., Auxietre, J.-L., Dunand, J.-P., Dupeuble, P.-A., and Mauffret, A. (1979). "The northwestern Iberian Margin: a Cretaceous passive margin deformed during Eocene," in *Deep drilling results in the Atlantic Ocean: continental margins and paleoenvironment* (Washington, D.C: American Geophysical Union), 138–153. doi:10.1029/ME003p0138

Boyer, D. L., and Zhang, X. (1990). Motion of oscillatory currents past isolated topography. *J. Phys. Oceanogr.* 20, 1425–1448. doi:10.1175/1520-0485(1990)020<1425:MOOCPI>2.0.CO;2

Brune, S., Heine, C., Clift, P. D., and Pérez-Gussinyé, M. (2017). Rifted margin architecture and crustal rheology: reviewing Iberia-Newfoundland, Central South Atlantic, and South China Sea. *Mar. Petroleum Geol.* 79, 257–281. doi:10.1016/j.marpetgeo.2016.10.018

Coxall, H. K., Huck, C. E., Huber, M., Lear, C. H., Legarda-Lisarri, A., O'Regan, M., et al. (2018). Export of nutrient rich Northern Component Water preceded early Oligocene Antarctic glaciation. *Nat. Geosci.* 11, 190–196. doi:10.1038/s41561-018-0069-9

Davies, R., Cartwright, J., Pike, J., and Line, C. (2001). Early Oligocene initiation of North Atlantic Deep Water formation. *Nature* 410, 917–920. doi:10.1038/35073551

de la Vara, A., and Meijer, P. (2016). Response of Mediterranean circulation to Miocene shoaling and closure of the Indian Gateway: a model study. *Palaeogeogr. Palaeoclimatol. Palaeoecol.* 442, 96–109. doi:10.1016/j.palaeo.2015.11.002

Dias, J. M. A., Gonzalez, R., Garcia, C., and Diaz-del-Rio, V. (2002a). Sediment distribution patterns on the Galicia-Minho continental shelf. *Prog. Oceanogr.* 52, 215–231. doi:10.1016/S0079-6611(02)00007-1

Dias, J. M. A., Jouanneau, J. M., Gonzalez, R., Araújo, M. F., Drago, T., Garcia, C., et al. (2002b). Present day sedimentary processes on the northern Iberian shelf. *Prog. Oceanogr.* 52, 249–259. doi:10.1016/S0079-6611(02)00009-5

Donnadieu, Y., Pucéat, E., Moiroud, M., Guillocheau, F., and Deconinck, J.-F. (2016). A better-ventilated ocean triggered by Late Cretaceous changes in continental configuration. *Nat. Commun.* 7, 10316. doi:10.1038/ncomms10316

Druet, M., Muñoz-Martín, A., Granja-Bruña, J. L., Carbó-Gorosabel, A., Acosta, J., Llanes, P., et al. (2018). Crustal structure and continent-ocean boundary along the Galicia continental margin (NW Iberia): insights from combined gravity and seismic interpretation. *Tectonics* 37, 1576–1604. doi:10.1029/2017TC004903

Duque-Caro, H. (1990). Neogene stratigraphy, paleoceanography and paleobiogeography in northwest South America and the evolution of the Panama seaway. *Palaeogeogr. Palaeoclimatol. Palaeoecol.* 77, 203–234. doi:10.1016/0031-0182(90)90178-A

Dutkiewicz, A., and Müller, R. D. (2022). Deep-sea hiatuses track the vigor of Cenozoic ocean bottom currents. *Geology* 50, 710–715. doi:10.1130/G49810.1

Ercilla, G., García-Gil, S., Estrada, F., Gràcia, E., Vizcaino, A., Váquez, J. T., et al. (2008). High-resolution seismic stratigraphy of the Galicia Bank Region and neighbouring abyssal plains (NW Iberian continental margin). *Mar. Geol.* 249, 108–127. doi:10.1016/j.margeo.2007.09.009

Faugères, J.-C., and Stow, D. A. V. (2008). "Chapter 14 contourite drifts: nature, evolution and controls," in *Contourites, developments in sedimentology*. Editors M. Rebesco, and A. Camerlenghi (Amsterdam, Netherlands: Elsevier), 257–288. doi:10.1016/S0070-4571(08)10014-0

Faugères, J.-C., Stow, D. A. V., Imbert, P., and Viana, A. (1999). Seismic features diagnostic of contourite drifts. *Mar. Geol.* 162, 1–38. doi:10.1016/S0025-3227(99)00068-7

Fiúza, A. F. G., Hamann, M., Ambar, I., del Rio, G. D., González, N., and Cabanas, J. M. (1998). Water masses and their circulation off western Iberia during May 1993. *Deep Sea Res. Part I Oceanogr. Res. Pap.* 45, 1127–1160. doi:10.1016/S0967-0637(98)00008-9

Galice, G., Auzende, J. P., Jonquet, H., and Olivet, J. L. (1979). "The continental margin off Galicia and Portugal: acoustical stratigraphy, dredge stratigraphy and structural evolution," in *Init. Rep. Deep sea drilling proj* (Washington: U.S. Government Printing Office), 633–662. doi:10.2973/dsdp.proc.47-2.133.1979

Hall, I. R., and McCave, I. N. (2000). Palaeocurrent reconstruction, sediment and thorium focussing on the Iberian margin over the last 140 ka. *Earth Planet. Sci. Lett.* 178, 151–164. doi:10.1016/S0012-821X(00)00068-6

Hanebuth, T. J. J., Alekseev, W., Andrade Grande, A., Baasch, B., Baumann, K.-H., Behrens, P., et al. (2012). Report and preliminary results of RV METEOR cruise M84/4, GALIOMAR III, Vigo - Vigo, 1st - 28th may, 2011. *Berichte, Fachbereich Geowissenschaften, Universität Bremen*, 1–139.

Hanebuth, T. J. J., Bender, V. B., Bujan, S., Elvert, M., Fredrichs, T., Kockisch, B., et al. (2007). Report and first results of the POSEIDON cruise P342 GALIOMAR, vigo-lisboa (Portugal), august 19th - september 06th, 2006. Distribution pattern, residence times and export of sediments on the pleistocene/holocene Galician shelf (NW Iberian Peninsula). *Berichte, Fachbereich Geowissenschaften, Universität Bremen* 255, 1–203.

Hanebuth, T. J. J., Zhang, W., Hofmann, A. L., Löwemark, L. A., and Schwenk, T. (2015). Oceanic density fronts steering bottom-current induced sedimentation deduced from a 50 ka contourite-drift record and numerical modeling (off NW Spain). *Quat. Sci. Rev.* 112, 207–225. doi:10.1016/j.quascirev.2015.01.027

Haug, G. H., and Tiedemann, R. (1998). Effect of the formation of the isthmus of Panama on Atlantic Ocean thermohaline circulation. *Nature* 393, 673–676. doi:10.1038/31447

Hayashi, T., Yamanaka, T., Hikasa, Y., Sato, M., Kuwahara, Y., and Ohno, M. (2020). Latest Pliocene Northern Hemisphere glaciation amplified by intensified Atlantic meridional overturning circulation. *Commun. Earth Environ.* 1, 25. doi:10.1038/s43247-020-00023-4

Hernández-Molina, F. J., Hüneke, H., Rodríguez-Tovar, F. J., Ng, Z. L., Llave, E., Mena, A., et al. (2022). Eocene to middle Miocene contourite deposits in Cyprus: a record of Indian Gateway evolution. *Glob. Planet. Change* 219, 103983. doi:10.1016/j.gloplacha.2022.103983

Hernández-Molina, F. J., Larter, R. D., Rebesco, M., and Maldonado, A. (2006). Miocene reversal of bottom water flow along the Pacific Margin of the Antarctic Peninsula: stratigraphic evidence from a contourite sedimentary tail. *Mar. Geol.* 228, 93–116. doi:10.1016/j.margeo.2005.12.010

Hernández-Molina, F. J., Serra, N., Stow, D. A. V., Llave, E., Ercilla, G., and Van Rooij, D. (2011). Along-slope oceanographic processes and sedimentary products around the Iberian margin. *Geo-Marine Lett.* 31, 315–341. doi:10.1007/s00367-011-0242-2

Hernández-Molina, F. J., Stow, D. A. V., Alvarez-Zarikian, C. A., Acton, G., Bahr, A., Balestra, B., et al. (2014). Onset of Mediterranean outflow into the North Atlantic. *Science* 344, 1244–1250. doi:10.1126/science.1251306

Hernández-Molina, F. J., Wåhlin, A., Bruno, M., Ercilla, G., Serra, N., Rosón, G., et al. (2016). Oceanographic processes and morphosedimentary products along the Iberian margins: a new multidisciplinary approach. *Mar. Geol.* 378, 127–156. doi:10.1016/j.margeo.2015.12.008

Hovikoski, J., Fyhn, M. B. W., Nøhr-Hansen, H., Hopper, J. R., Andrews, S., Barham, M., et al. (2021). Paleocene-Eocene volcanic segmentation of the Norwegian-Greenland seaway reorganized high-latitude ocean circulation. *Commun. Earth Environ.* 2, 172. doi:10.1038/s43247-021-00249-w

Jovane, L., Coccioni, R., Marsili, A., and Acton, G. (2009). "The late Eocene greenhouse-icehouse transition: observations from the Massignano global stratotype section and point (GSSP)," in *The late Eocene earth—hothouse, icehouse, and impacts*. Editors C. Koeberl, and A. Montanari (Boulder, Colorado: Geological Society of America). doi:10.1130/2009.2452(10

Jovane, L., Florindo, F., and Dinarès-Turell, J. (2004). Environmental magnetic record of paleoclimate change from the Eocene-Oligocene stratotype section, Massignano, Italy. *Massignano, Italy. Geophys. Res. Lett.* 31. doi:10.1029/2004GL020554

Karas, C., Nürnberg, D., Bahr, A., Groeneveld, J., Herrle, J. O., Tiedemann, R., et al. (2017). Pliocene oceanic seaways and global climate. *Sci. Rep.* 7, 39842. doi:10.1038/srep39842

King, M. T., Welford, J. K., and Peace, A. L. (2020). Investigating the role of the Galicia Bank on the formation of the North West Iberian margin using deformable plate tectonic models. *Tectonophysics* 789, 228537. doi:10.1016/j.tecto.2020.228537

Knutz, P. C. (2008). "Chapter 24 palaeoceanographic significance of contourite drifts," in *Contourites, developments in sedimentology*. Editors M. Rebesco, and A. Camerlenghi (Amsterdam, Netherlands: Elsevier), 511–535. doi:10.1016/S0070-4571(08)10024-3

Kouwenhoven, T. J., and van der Zwaan, G. J. (2006). A reconstruction of late Miocene Mediterranean circulation patterns using benthic foraminifera. *Palaeogeogr. Palaeoclimatol. Palaeoecol.* 238, 373–385. doi:10.1016/j.palaeo.2006.03.035

Lagabrielle, Y., Goddéris, Y., Donnadieu, Y., Malavieille, J., and Suarez, M. (2009). The tectonic history of Drake Passage and its possible impacts on global climate. *Earth Planet. Sci. Lett.* 279, 197–211. doi:10.1016/j.epsl.2008.12.037

Langton, S. J., Rabideaux, N. M., Borrelli, C., and Katz, M. E. (2016). Southeastern Atlantic deep-water evolution during the late-middle Eocene to earliest Oligocene (ocean drilling program site 1263 and deep sea drilling Project site 366). *Geosphere* 12, 1032–1047. doi:10.1130/GES01268.1

Lantzsch, H., Hanebuth, T. J. J., and Bender, V. B. (2009). Holocene evolution of mud depocentres on a high-energy, low-accumulation shelf (NW Iberia). *Quat. Res.* 72, 325–336. doi:10.1016/j.yqres.2009.07.009

Lantzsch, H., Hanebuth, T. J. J., and Henrich, R. (2010). Sediment recycling and adjustment of deposition during deglacial drowning of a low-accumulation shelf (NW Iberia). *Cont. Shelf Res.* 30, 1665–1679. doi:10.1016/j.csr.2010.06.013

Le Pichon, X., and Sibuet, J.-C. (1971). Western extension of boundary between European and Iberian plates during the Pyrenean orogeny. *Earth Planet. Sci. Lett.* 12, 83–88. doi:10.1016/0012-821X(71)90058-6

Liu, S., Hernández-Molina, F. J., Rodrigues, S., and Van Rooij, D. (2023). Deep-water circulation in the northeast Atlantic during the mid- and late cretaceous. *Geology* 51, 515–520. doi:10.1130/G50886.1

López-Pérez, A. E., Rubio, B., Rey, D., Plaza-Morlote, M., and Pinheiro, L. M. (2021). Late Quaternary tectono-sedimentary processes on an isolated offshore high marginal platform (NW Iberian Continental Margin). *Mar. Geol.* 431, 106374. doi:10.1016/j.margeo.2020.106374

Martín-González, F., and Heredia, N. (2011). Geometry, structures and evolution of the western termination of the Alpine-Pyrenean Orogen reliefs (NW Iberian Peninsula). *J. Iber. Geol.* 37, 103–120. doi:10.5209/rev_JIGE.2011.v37.n2.1

Martins, V. A., Santos, J. F., Mackensen, A., Dias, J. A., Ribeiro, S., Moreno, J. C., et al. (2013). The sources of the glacial IRD in the NW Iberian Continental Margin over the last 40 ka. *Quat. Int.* 318, 128–138. doi:10.1016/j.quaint.2013.08.026

McCave, I. N., and Hall, I. R. (2002). Turbidity of waters over the Northwest Iberian continental margin. *Prog. Oceanogr.* 52, 299–313. doi:10.1016/S0079-6611(02)00012-5

Mena, A., Francés, G., Pérez-Arlucea, M., Hanebuth, T. J. J., Bender, V. B., and Nombela, M. A. (2018). Evolution of the Galicia Interior Basin over the last 60 ka: sedimentary processes and palaeoceanographic implications. *J. Quat. Sci.* 33, 536–549. doi:10.1002/jqs.3032

Mienert, J., Flood, R. D., and Dullo, W. C. (1994). Research perspectives of sediment waves and drifts: monitors of global change in deepwater circulation. *Paleoceanography* 9, 893–895. doi:10.1029/94PA02117

Miller, K. G., Wright, J. D., Katz, M. E., Wade, B. S., Browning, J. V., Cramer, B. S., et al. (2009). "Climate threshold at the Eocene-Oligocene transition: Antarctic ice sheet influence on ocean circulation," in *The late Eocene earth—hothouse, icehouse, and impacts* (Boulder, Colorado: Geological Society of America). doi:10.1130/2009.2452(11

Montes, C., Cardona, A., Jaramillo, C., Pardo, A., Silva, J. C., Valencia, V., et al. (2015). Middle Miocene closure of the Central American Seaway. *Science* 348, 226–229. doi:10.1126/science.aaa2815

Muñoz, A., Acosta, J., and Uchupi, E. (2003). Cenozoic tectonics on the Galicia margin, northwest Spain. *Geo-Marine Lett.* 23, 72–80. doi:10.1007/s00367-003-0126-1

Murillas, J., Mougenot, D., Boulot, G., Comas, M. C., Banda, E., and Mauffret, A. (1990). Structure and evolution of the Galicia Interior Basin (Atlantic western iberian continental margin). *Tectonophysics* 184, 297–319. doi:10.1016/0040-1951(90)90445-E

Murphy, D. P., and Thomas, D. J. (2013). The evolution of Late Cretaceous deep-ocean circulation in the Atlantic basins: neodymium isotope evidence from South Atlantic drill sites for tectonic controls. *Geochem. Geophys. Geosyst.* 14, 5323–5340. doi:10.1002/2013GC004889

Newkirk, D. R., and Martin, E. E. (2009). Circulation through the Central American Seaway during the Miocene carbonate crash. *Geology* 37, 87–90. doi:10.1130/G25193A.1

Ng, Z. L., Hernández-Molina, F. J., Duarte, D., Sierro, F. J., Ledesma, S., Rogerson, M., et al. (2021). Latest Miocene restriction of the Mediterranean Outflow Water: a perspective from the Gulf of Cádiz. *Geo-Mar Lett.* 41, 23. doi:10.1007/s00367-021-00693-9

Nielsen, T., Knutz, P. C., and Kuijpers, A. (2008). "Chapter 16 seismic expression of contourite depositional systems," in *Contourites, developments in sedimentology*. Editors M. Rebesco, and A. Camerlenghi (Amsterdam, Netherlands: Elsevier), 301–321. doi:10.1016/S0070-4571(08)10016-4

Nisancioglu, K., Raymo, M., and Stone, P. (2003). Reorganization of Miocene deep water circulation in response to the shoaling of the Central American Seaway. *Paleoceanography* 18. doi:10.1029/2002PA000767

Oberle, F. K. J., Hanebuth, T. J. J., Baasch, B., and Schwenk, T. (2014a). Volumetric budget calculation of sediment and carbon storage and export for a late Holocene mid-shelf mudbelt system (NW Iberia). *Cont. Shelf Res.* 76, 12–24. doi:10.1016/j.csr.2013.12.012

Oberle, F. K. J., Storlazzi, C. D., and Hanebuth, T. J. J. (2014b). Wave-driven sediment mobilization on a storm-controlled continental shelf (Northwest Iberia). *J. Mar. Syst.* 139, 362–372. doi:10.1016/j.jmarsys.2014.07.018

O'Dea, A., Lessios, H. A., Coates, A. G., Eytan, R. I., Restrepo-Moreno, S. A., Cione, A. L., et al. (2016). Formation of the Isthmus of Panama. *Sci. Adv.* 2, e1600883. doi:10.1126/sciadv.1600883

Oliveira, A., Vitorino, J., Rodrigues, A., Jouanneau, J. M., Dias, J. A., and Weber, O. (2002). Nepheloid layer dynamics in the northern Portuguese shelf. *Prog. Oceanogr.* 52, 195–213. doi:10.1016/S0079-6611(02)00006-X

Palcu, D. V., Muraszko, J. R., Jaqueto, P. F., and Jovane, L. (2020). The birth of a connected South Atlantic Ocean: a magnetostratigraphic perspective. *Front. Earth Sci.* 8. doi:10.3389/feart.2020.00375

Pérez-Asensio, J. N., Aguirre, J., Schmiedl, G., and Civis, J. (2012). Impact of restriction of the Atlantic-Mediterranean gateway on the Mediterranean Outflow Water and eastern Atlantic circulation during the Messinian. *Paleoceanography* 27. doi:10.1029/2012PA002309

Pérez-Díaz, L., and Eagles, G. (2017). South Atlantic paleobathymetry since early Cretaceous. *Sci. Rep.* 7, 11819. doi:10.1038/s41598-017-11959-7

Pérez-Gussinyé, M., Ranero, C. R., Reston, T. J., and Sawyer, D. (2003). Mechanisms of extension at nonvolcanic margins: evidence from the Galicia interior basin, west of Iberia. *J. Geophys. Res. Solid Earth* 108. doi:10.1029/2001JB000901

Petrovic, A., Lantzsch, H., Schwenk, T., Marquardt, J., Titschack, J., and Hanebuth, T. J. J. (2019). Post-LGM upward shift of the Mediterranean Outflow Water recorded in a contourite drift off NW Spain. *Mar. Geol.* 407, 334–349. doi:10.1016/j.margeo.2018.11.015

Plaza-Morlote, M., Rey, D., Santos, J. F., Ribeiro, S., Heslop, D., Bernabeu, A., et al. (2017). Southernmost evidence of large European ice sheet-derived freshwater discharges during the Heinrich Stadials of the Last Glacial Period (Galician Interior Basin, northwest iberian continental margin). *Earth Planet. Sci. Lett.* 457, 213–226. doi:10.1016/j.epsl.2016.10.020

Poore, H. R., Samworth, R., White, N. J., Jones, S. M., and McCave, I. N. (2006). Neogene overflow of Northern Component Water at the Greenland-Scotland Ridge. *Geochem. Geophys. Geosystems* 7. doi:10.1029/2005GC001085

Preu, B., Schwenk, T., Hernández-Molina, F. J., Violante, R., Paterlini, M., Krastel, S., et al. (2012). Sedimentary growth pattern on the northern Argentine slope: the impact of North Atlantic Deep Water on southern hemisphere slope architecture. *Mar. Geol.* 329 (331), 113–125. doi:10.1016/j.margeo.2012.09.009

Pucéat, E., Lécuyer, C., and Reisberg, L. (2005). Neodymium isotope evolution of NW Tethyan upper ocean waters throughout the Cretaceous. *Earth Planet. Sci. Lett.* 236, 705–720. doi:10.1016/j.epsl.2005.03.015

Raymo, M. E., Hodell, D., and Jansen, E. (1992). Response of deep ocean circulation to initiation of northern hemisphere glaciation (3–2 MA). *Paleoceanography* 7, 645–672. doi:10.1029/92PA01609

Rebesco, M., Hernández-Molina, F. J., Van Rooij, D., and Wåhlin, A. (2014). Contourites and associated sediments controlled by deep-water circulation processes: state-of-the-art and future considerations. *Mar. Geol.* 352, 111–154. doi:10.1016/j.margeo.2014.03.011

Robinson, S. A., and Vance, D. (2012). Widespread and synchronous change in deep-ocean circulation in the North and South Atlantic during the Late Cretaceous. *Paleoceanography* 27. doi:10.1029/2011PA002240

Rogerson, M., Rohling, E. J., Bigg, G. R., and Ramirez, J. (2012). Paleoceanography of the Atlantic-Mediterranean exchange: overview and first quantitative assessment of climatic forcing. *Rev. Geophys.* 50. doi:10.1029/2011RG000376

Rögl, F. (1999). Mediterranean and Paratethys. Facts and hypotheses of an Oligocene to Miocene paleogeography (short overview). *Geol. carpathica* 50, 339–349.

Roque, C., Hernández-Molina, J., Brito, P., Madureira, P., Quartau, R., Magalhães, V., et al. (2023). Contourite depositional systems offshore Madeira island: decoding the deepwater circulation since the Late Cretaceous to the Quaternary in the NE-Central Atlantic. *Glob. Planet. Change* 225, 104118. doi:10.1016/j.gloplacha.2023.104118

Roth, P. H. (1986). Mesozoic palaeoceanography of the North Atlantic and Tethys Oceans. *Geol. Soc. Lond. Spec. Publ.* 21, 299–320. doi:10.1144/GSL.SP.1986.021.01.22

Sandoval, L., Welford, J. K., MacMahon, H., and Peace, A. L. (2019). Determining continuous basins across conjugate margins: the East Orphan, Porcupine, and Galicia Interior Basins of the southern North Atlantic ocean. *Mar. Petroleum Geol.* 110, 138–161. doi:10.1016/j.marpetgeo.2019.06.047

Scher, H. D., and Martin, E. E. (2004). Circulation in the Southern Ocean during the Paleogene inferred from neodymium isotopes. *Earth Planet. Sci. Lett.* 228, 391–405. doi:10.1016/j.epsl.2004.10.016

Scher, H. D., and Martin, E. E. (2006). Timing and Climatic Consequences of the Opening of Drake Passage. *Science* 312, 428–430. doi:10.1126/science.1120044

Scher, H. D., and Martin, E. E. (2008). Oligocene deep water export from the North Atlantic and the development of the Antarctic Circumpolar Current examined with neodymium isotopes. *Paleoceanography* 23. doi:10.1029/2006PA001400

Schönfeld, J., and Zahn, R. (2000). Late Glacial to Holocene history of the Mediterranean Outflow. Evidence from benthic foraminiferal assemblages and stable isotopes at the Portuguese margin. *Palaeogeogr. Palaeoclimatol. Palaeoecol.* 159, 85–111. doi:10.1016/S0031-0182(00)00035-3

Sclater, J. G., and Christie, P. A. F. (1980). Continental stretching: an explanation of the Post-Mid-Cretaceous subsidence of the central North Sea Basin. *J. Geophys. Res. Solid Earth* 85, 3711–3739. doi:10.1029/JB085iB07p03711

Sewall, J. O., van de Wal, R. S. W., van der Zwan, K., van Oosterhout, C., Dijkstra, H. A., and Scotese, C. R. (2007). Climate model boundary conditions for four Cretaceous time slices. *Clim. Past.* 3, 647–657. doi:10.5194/cp-3-647-2007

Soares, D. M., Alves, T. M., and Terrinha, P. (2014). Contourite drifts on early passive margins as an indicator of established lithospheric breakup. *Earth Planet. Sci. Lett.* 401, 116–131. doi:10.1016/j.epsl.2014.06.001

Stille, P., Steinmann, M., and Riggs, S. R. (1996). Nd isotope evidence for the evolution of the paleocurrents in the Atlantic and Tethys Oceans during the past 180 Ma. *Earth Planet. Sci. Lett.* 144, 9–19. doi:10.1016/0012-821X(96)00157-4

Stow, D. A. V., Hernández-Molina, F. J., Alvarez Zarikian, C. A., and Expedition 339 Scientists (2013). *Mediterranean outflow, proceedings of the IODP.* Lisbon, Portugal: International Ocean Discovery Program. doi:10.2204/iodp.proc.339.2013

Stow, D. A. V., Hernández-Molina, F. J., Llave, E., Sayago-Gil, M., Díaz del Río, V., and Branson, A. (2009). Bedform-velocity matrix: the estimation of bottom current velocity from bedform observations. *Geology* 37, 327–330. doi:10.1130/G25259A.1

Stow, D. A. V., Hunter, S., Wilkinson, D., and Hernández-Molina, F. J. (2008). "Chapter 9 the nature of contourite deposition," in *Contourites, developments in sedimentology.* Editors M. Rebesco and A. Camerlenghi (Amsterdam, Netherlands: Elsevier), 143–156. doi:10.1016/S0070-4571(08)10009-7

Straume, E. O., Gaina, C., Medvedev, S., and Nisancioglu, K. H. (2020). Global cenozoic paleobathymetry with a focus on the northern hemisphere oceanic gateways. *Gondwana Res.* 86, 126–143. doi:10.1016/j.gr.2020.05.011

Sutra, E., and Manatschal, G. (2012). How does the continental crust thin in a hyperextended rifted margin? Insights from the Iberia margin. *Geology* 40, 139–142. doi:10.1130/G32786.1

Thomas, D. J., Bralower, T. J., and Jones, C. E. (2003). Neodymium isotopic reconstruction of late Paleocene–early Eocene thermohaline circulation. *Earth Planet. Sci. Lett.* 209, 309–322. doi:10.1016/S0012-821X(03)00096-7

Torfstein, A., and Steinberg, J. (2020). The Oligo–Miocene closure of the Tethys Ocean and evolution of the proto-Mediterranean Sea. *Sci. Rep.* 10, 13817. doi:10.1038/s41598-020-70652-4

Trabucho Alexandre, J., Tuenter, E., Henstra, G. A., van der Zwan, K. J., van de Wal, R. S. W., Dijkstra, H. A., et al. (2010). The mid-Cretaceous North Atlantic nutrient trap: black shales and OAEs. *Paleoceanography* 25. doi:10.1029/2010PA001925

Tremblin, M., Hermoso, M., and Minoletti, F. (2016). Equatorial heat accumulation as a long-term trigger of permanent Antarctic ice sheets during the Cenozoic. *Proc. Natl. Acad. Sci.* 113, 11782–11787. doi:10.1073/pnas.1608100113

Uenzelmann-Neben, G., and Gruetzner, J. (2018). Chronology of Greenland Scotland Ridge overflow: what do we really know? *Mar. Geol.* 406, 109–118. doi:10.1016/j.margeo.2018.09.008

Uenzelmann-Neben, G., Weber, T., Grützner, J., and Thomas, M. (2017). Transition from the Cretaceous ocean to Cenozoic circulation in the western South Atlantic — a twofold reconstruction. *Tectonophysics* 716, 225–240. doi:10.1016/j.tecto.2016.05.036

Van Rooij, D., Iglesias, J., Hernández-Molina, F. J., Ercilla, G., Gomez-Ballesteros, M., Casas, D., et al. (2010). The Le Danois Contourite Depositional System: Interactions between the Mediterranean Outflow Water and the upper Cantabrian Slope (North Iberian margin). *Mar. Geol.* 274, 1–20. doi:10.1016/j.margeo.2010.03.001

Varela, R. A., Rosón, G., Herrera, J. L., Torres-López, S., and Fernández-Romero, A. (2005). A general view of the hydrographic and dynamical patterns of the Rías Baixas adjacent sea area. *J. Mar. Syst.* 54, 97–113. doi:10.1016/j.jmarsys.2004.07.006

Vázquez, J. T., Medialdea, T., Ercilla, G., Somoza, L., Estrada, F., Puga, M. C. F., et al. (2008). Cenozoic deformational structures on the Galicia Bank region (NW iberian continental margin). *Mar. Geol.* 249, 128–149. doi:10.1016/j.margeo.2007.09.014

Via, R. K., and Thomas, D. J. (2006). Evolution of Atlantic thermohaline circulation: early Oligocene onset of deep-water production in the North Atlantic. *Geology* 34, 441–444. doi:10.1130/G22545.1

Vitorino, J., Oliveira, A., Jouanneau, J. M., and Drago, T. (2002). Winter dynamics on the northern Portuguese shelf. Part 2: bottom boundary layers and sediment dispersal. *Prog. Oceanogr.* 52, 155–170. doi:10.1016/S0079-6611(02)00004-6

Voelker, A. H. L., Lebreiro, S. M., Schönfeld, J., Cacho, I., Erlenkeuser, H., and Abrantes, F. (2006). Mediterranean outflow strengthening during northern hemisphere coolings: a salt source for the glacial Atlantic? *Earth Planet. Sci. Lett.* 245, 39–55. doi:10.1016/j.epsl.2006.03.014

Wilckens, H., Eggenhuisen, J. T., Adema, P. H., Hernández-Molina, F. J., Jacinto, R. S., and Miramontes, E. (2023a). Secondary flow in contour currents controls the formation of moat-drift contourite systems. *Commun. Earth Environ.* 4, 316. doi:10.1038/s43247-023-00978-0

Wilckens, H., Schwenk, T., Lüdmann, T., Betzler, C., Zhang, W., Chen, J., et al. (2023b). Factors controlling the morphology and internal sediment architecture of moats and their associated contourite drifts. *Sedimentology* 70, 1472–1495. doi:10.1111/sed.13093

Willeit, M., Ganopolski, A., Calov, R., and Brovkin, V. (2019). Mid-Pleistocene transition in glacial cycles explained by declining CO_2 and regolith removal. *Sci. Adv.* 5, eaav7337. doi:10.1126/sciadv.aav7337

Woodruff, F., and Savin, S. M. (1989). Miocene deepwater oceanography. *Paleoceanography* 4, 87–140. doi:10.1029/PA004i001p00087

Wright, J. D., Miller, K. G., and Fairbanks, R. G. (1992). Early and middle Miocene stable isotopes: implications for deepwater circulation and climate. *Paleoceanography* 7, 357–389. doi:10.1029/92PA00760

Zhang, W., Cui, Y., Santos, A. I., and Hanebuth, T. J. J. (2016a). Storm-driven bottom sediment transport on a high-energy narrow shelf (NW Iberia) and development of mud depocenters. *J. Geophys. Res. Oceans* 121, 5751–5772. doi:10.1002/2015JC011526

Zhang, W., Hanebuth, T. J. J., and Stöber, U. (2016b). Short-term sediment dynamics on a meso-scale contourite drift (off NW Iberia): impacts of multi-scale oceanographic processes deduced from the analysis of mooring data and numerical modelling. *Mar. Geol.* 378, 81–100. doi:10.1016/j.margeo.2015.12.006